

Regional Seismic Information Entropy for Detecting Precursors of Earthquake Activation

Yukio Ohsawa

Department of Systems Innovation, School of Engineering, The University of Tokyo (Japan),
Postal address: 7-3-1 Hongo, Bunkyo-ku Tokyo 113-8656 Japan [ohsawa -at- sys.t.u-tokyo.ac.jp]

Abstract: Here a method is presented for detecting precursors of earthquakes from time series data on earthquakes in a target region. Regional Entropy of Seismic Information, a quantity representing the average influence of an earthquake in the target region to the diversity of clusters to which earthquakes distribute, is introduced. Based on a rough qualitative model of the dynamics of land crust, it is hypothesized that the saturation after the increase in the Regional Entropy of Seismic Information precedes the activation of earthquakes. On the open earthquake catalog, this hypothesis is validated. This temporal change turned out to correlate more with the activation of earthquakes in Japanese regions, by one to two years precedence, than the compared baseline methods.

Introduction

Methods for detecting precursors of earthquakes have been invented from the aspect of sciences on the earth. The complex dynamics of the land crust and its interaction with fluid have been studied, for modeling precursory events of earthquakes such as nucleation, dilatancy, and colliding cascade^{1,2}. By also integrating changes in wave velocity and strain, electromagnetic phenomena, and even behaviors of animals, methods for the detection of earthquake precursors have been developed and integrated establishing sciences on complex systems^{3,4,5,6}. From the approach to measure the local seismicity of each region, the appearance of seismic gaps, regions where earthquakes are less frequent than the expectation based on the seismicity in the surrounding regions, may be regarded as a candidate of precursor^{1,7}. The size of a seismic gap where precursors are expected, called an earthquake preparation zone, have been estimated on the deformation and the tilts at the surface of the earth⁸.

On the other hand, purely data-driven approaches with the development of computing algorithms are also addressed to earthquake prediction⁹⁻¹³. For example, the eigenvectors and their corresponding eigenvalues, of the $N \times N$ matrix representing the pairwise co-occurrences of earthquakes in N regions, have been used to predict the probability of earthquakes in clusters of regions¹³. Machine learning techniques for detecting the change in some change point score¹⁴⁻¹⁶, based on the transition of models on latent dynamics from before and after time t , may also have a potential to discover an essential change of the land crust behavior. However, the precursors of large earthquakes have been hard to capture from this approach due to the complex unknown latent dynamics and the extremely low frequency of the target event. For example, the frequency of M8.0 events is incomparably lower than of M4.0, and the precursor of the former may differ from the latter because it may be caused by active faults in the larger range of land crust or the large-scale tectonic dynamics. Thus, M8.0 cannot be predicted by learning patterns from the large data on the large amount of M4.0 earthquakes.

Generally, such a data-driven approach, if applied without any model of the dynamics of the earth, hardly works in forecasting or explaining events called “unexpected” after occurrence, e.g., earthquakes of M7.3 in

South-Hyogo in Japan (1995)¹⁷, M9.0 in North-East Japan (2011)¹⁸, M7.9 in Sichuan province of China (2008)¹⁹, and M5.3 of Washington DC (2011)²⁰. For example, the M7.3 in South-Hyogo occurred on a known and mapped fault by an unexpected timing; the M 9.0 North-East Japan earthquake occurred in the range where scientists expected, but by a larger magnitude than anticipated. As far as we go on the specifications and/or the extensions of the idea to learn patterns or parameters ruling the patterns from data, the expectation based on the learned pattern cannot cover real events which are not preceded by the condition corresponding to any learned pattern. In general, data-based approaches in seismology have been basically applied for regions of considerably frequent earthquakes, but their mathematic models should be integrated with some causality model of earthquakes for forecasting the occurrence of large earthquakes in regions where the frequency of large earthquakes was low or in the surrounding regions.

On the discussion above, data analysis based on models or knowledge in seismology can be regarded as a reasonable direction. For example, the value of coefficient b in Gutenberg-Richter's (GR) equation^{3,21}, computed from the data on earthquakes of each year in the target region, decreases for such a period as 10 years before the increase in the frequency of large ($M > 6.2$) earthquakes. However, in using this knowledge for detecting a precursor, the computed value has been found to be unreliable in the ranges of small or large magnitude of earthquakes. Furthermore, the changing period of 10 years means this is the time resolution we can expect in prediction. On the other hand, statistic models of earthquake occurrence in space-and-time, an earthquake at each location at each time came to be modeled as the effect of previous events that in the target region and also in surrounding areas²²⁻²⁴. In the literature of probabilistic forecasting²² of earthquakes, prediction within an error of 10 years came to be realized for regions of frequent earthquakes such as the North-West and the Sout-West Pacific Oceans. Epidemic Type Aftershock Sequence (ETAS)²³ also shows a good performance at estimating the risk in regions of frequent earthquakes and has been extended to predicting earthquakes of maximum magnitudes²⁴. However, some earthquakes beyond the reach of these models show great exposures of energy, especially in regions where the frequency of earthquakes is low. For example, the focus of Kumamoto earthquake (M7.3) in 2016 or of Osaka (M6.1) in 2018 are not captured as high-risk regions of M7.0 or M6.0 by the extended ETAS²⁴.

Other models for the predictive analysis of data are found to be relevant to models in geophysics, such as theories of renormalization group and of nonlinear system²⁵. Keilis-Borok etc. modeled earthquakes as events in a non-linear system, on which they enabled algorithmic data-based extraction of premonitory patterns of earthquakes^{5, 26-29}. Their composite algorithm used a combination of patterns for predicting earthquakes in various regions. For example, the algorithm CN was developed by retrospective analysis of seismicity preceding large earthquakes²⁹. Here the time of increased probability (TIP) of strong earthquakes has been diagnosed using functions representing the levels of the seismic activity, the quiescence, the temporal variation of seismicity, the spatial concentration, the clustering of earthquakes, the spatial contrast of activity, and the long-range interaction of earthquakes. The interaction and the variety of earthquake activities across a wide region have been also considered in the approach of pattern informatics (PI^{30,31}). An earthquake is here assumed to be a multi-body phenomenon ruled by latent dynamics of lithosphere on a load plate, interacting to form a threshold system^{32, 33}. The value of PI index for a region, corresponding to the difference in the intensity-growth from the background regions, have been found to provide forecasts of locations and the magnitude of upcoming earthquakes within an error of 10 years for various regions³⁴⁻³⁸. Relative Intensity^{34,36,39}, in spite of the simplicity of computation, has been compared with (outperforming in some cases⁴⁰) PI in the performance to detect precursors.

In this paper, the author stands on data science rather than of seismology, in that the focus is to find precursors of earthquakes from data available in an earthquake catalog. Nevertheless, as discussed above, we should take some (at least a rough) model of earthquake dynamics into account, in order to forecast the unexpected activation of earthquakes. Here we borrow the idea of a cluster-based analysis of data from earthquake catalog⁴¹, where the co-occurrence of earthquakes has been used for extracting not only the clusters

of active faults quaking at close times but also the interrelationships among multiple clusters. In this previous work, some regions of low earthquake frequency have been highlighted as of near-future risks and coincided with the locations of real events. This method can be said to be based on a rough model of earthquakes, assuming that such a region may be stressed by the movements of multiple clusters of active faults. However, the information about temporal changes in the data is dropped as far as the method relies on the co-occurrences as a statistic quantity. In this paper, for detecting a short-term (preceding 1 or 2 years) precursor of the activation of earthquakes in a target region, a quantitative index called Regional Entropy of Seismic Information (RESI) is proposed. RESI is based on a rough model of land crust dynamics proposed in the next section, that extends the idea of inter-cluster interaction⁴¹ by introducing the temporal changing of clusters' structure. The performance of this index in detecting precursors of earthquakes is evaluated on the open data of earthquake catalog.

The restructuring of clusters of foci as a rough model of the precursory process of earthquake activation

Let us introduce a rough model of land crust dynamics, as the basis of the model for data analysis proposed later. The model assumes the transitions from the state (a) or (b) to (e) illustrated in Fig 1 in the whole geographical region S^U covered by the target data, roughly composed of the two phases below. In this rough model, we investigate the dynamic restructuring of clusters and inter-cluster interaction of earthquake foci (approximated by “quaking meshes” of as stated later), including their separation/combination and the activation/deactivation of earthquakes in them, based on data about the time and the location of each earthquake.

Phase 1: The diversity of clusters, to which earthquakes distribute, increases from state (a) or (b) in Fig.1 to state (c). Here a cluster gets separated to make a seismic gap as in Fig 1 (c) due to the local disappearing of earthquakes in the central part of (a), or the appearance of a new cluster close to the existed one such as (b).

Phase 2: Earthquakes converge to a fewer clusters, as from Fig.1 (c) to (e), possibly via state (d). Here, the clusters of foci get combined as in (e) due to earthquakes to occur in the seismic gap in (c). In this step, the tentative seismic gap as in (c) comes to be the preparation zone, to have earthquakes in the transition to (e). Before reaching the state (e), earthquakes may occur in the seismic gap and the state moves from/to (d) and (e), during the transition period. If (e) is reached, the clusters linked via the bridge get combined and the value of entropy defined in Eq.(1) below decreases. Here, S is the target region to compute the entropy for, that is the whole region S^U here, and C_i is the i -th cluster of earthquake foci in S .

$$H(S, t) = \sum_i p(C_i|S, t) \log p(C_i|S, t) \quad (1)$$

Here, in order to capture the dynamics above, the traditional information entropy⁴² $H(S, t)$ of region S at time t is expressed in terms of a discrete set of probabilities $p(C_i|S, t)$ for discrete microstates. The i -th microstate is interpreted as the i -th cluster C_i of foci in region S , to which the focus of each earthquake may belong. The definition of a cluster here will be given later in Step 1 of the proposed algorithm and can be intuitively understood as a group of closely located foci of earthquakes in a period (e.g., a month or a year).

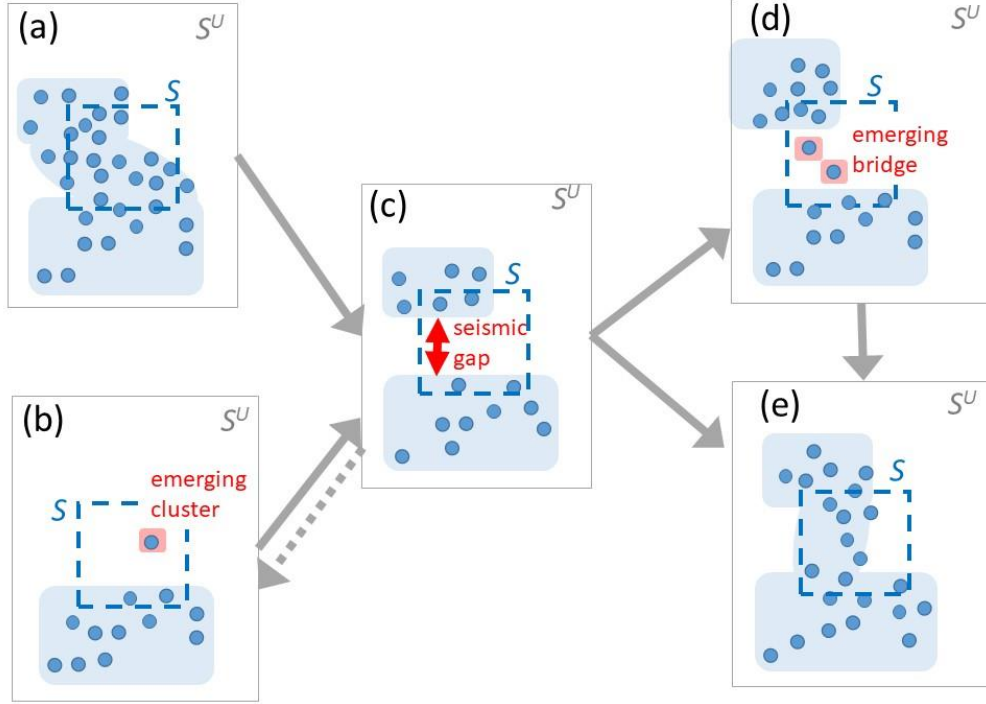


Figure 1. Transitions of earthquake activation. In each state from (a) through (e), the appearance of seismic gaps and the bridges are regarded as a candidate of precursor of earthquake activation. Each earthquake in a sparse region is illustrated to form one cluster in (b) and (d).

For region S^U , corresponding to each snapshot in Fig.1, the value of $H(S^U)$ increases in the transition from the state (a) or (b) to (c), and then decreases from the state (c) to (e). It is possible that earthquakes in one of the clusters in (c) disappear, that is a pattern of decrease in $H(S^U)$. In this paper, such a case is regarded as a transition in the dotted arrow from (c) to (b), followed by returning to (c) before the occurrence of a large earthquake. Thus, as state (c) in Fig.1 is originated from such as state as (a) or (b), corresponding to the increase in the entropy of region S^U , state (c) is here assumed to imply a precursor of the activation of earthquakes in all the transition paths considered here i.e., from $\{(a) \text{ or } (b)\}$ to/from (c) and then to (d) or (e).

Although this assumption is rough for modeling real dynamics of earthquakes, we expect the roughness absorbs the differences of the dynamics of various earthquakes. For example, the deeper earthquakes on the dipping interface of subduction plates and the shallower ones at active faults in the inland are ruled by different dynamics. If we apply fine models for analyzing the activities of land crust reflecting the difference of dynamics, we should build various models and also a hybrid model if earthquakes occur from the mixture of dynamics.

A note about entropy

Note that the entropy introduced here is not exactly the one used in statistical physics or statistical mechanics⁴³, or its application to understanding earthquakes⁴⁴, but the one in information science. In statistical physics, entropy has been defined, with being related to the numbers of microscopic configurations of a thermodynamic system, specified by some macroscopic variables. For example, entropy can be specified by the physical parameter of the system as energy divided by temperature in thermodynamics. In statistical mechanics, entropy is a measure of the number of ways in which a system may be arranged, quantified by the average logarithm of the number of possible microscopic configurations of the particles in the system, observed as the macroscopic

disorder of the system. On the other hand, in information science, entropy is the sheer amount of information needed to specify the full set of microstates of the system, which is not specified by a macroscopic variable. In this paper, entropy means the one in information science with taking a cluster, to which an earthquake may belong, as a microstate. Thus, entropy here is defined to quantify the diversity of clusters of “quaking meshes” that are meshes of the land including foci in the target region. It should be also noted the proposed method is to compute entropy based on clusters, not using entropy as a criterion for clustering as in the literature⁴⁵.

Also, let us position this method in the history of applying entropy in information science⁴². Entropy in information science has been used for quantifying the diversity of events in target systems. In marketing, entropy has been used as an index of diversity of interests and products⁴⁶⁻⁴⁸. In digital images, the temporal change of entropy for each part of a given image has been used in detecting contours and their movements⁴⁹. Furthermore, entropies in traffics and events in computer networks turned out to provide a scalable technique to detect unexpected behaviors and abrupt changes^{50, 51}. In this history, the contribution of this paper is to couple the computation of entropy with a method for clustering foci, and to consider the average influence of every single earthquake in a region to the entropy of the universe, i.e., the whole given map.

Regional Entropy of Seismic Information

The definition

On the assumption above, let us here model the dynamics of clusters’ restructuring as from (a) through (e) in Fig 1, introducing Regional Entropy of Seismic Information (RESI in short) $Hr(S, t)$ in Eq. (2).

$$Hr(S, t) = H(S, t) - \log p(S, t) \quad (2)$$

Here, $H(S, t)$ is given by $\sum_{C \in \text{Msh}(S)} p(C|S, t) \log p(C|S, t)$ that is an approximation by replacing the foci in Eq.(1) by the meshes in $\text{Msh}(S)$, where $\text{Msh}(S)$ is the set of meshes of land including foci in S . Intuitively, by $Hr(S, t)$ the author is meaning the average contribution per earthquake in region S to the diversity of clusters of foci. Here, locations of foci are approximated by quaking meshes, i.e., the meshes of the land including foci of earthquakes. Also, note we approximate the 3D location of foci of earthquakes by 2D ignoring the depth. Although considering the depth is basically expected to improve the performance of the presented method, here we thus approximate for comparing fairly with baseline methods that essentially use 2D information in the data, in the experimental section. That is, quaking meshes are the meshes of including epicenters.

$Hr(S, t)$ in Eq.(2) can be rewritten as $\sum_{C \in \text{Msh}(S)} p(C, t) \log p(C, t)$ divided by $p(S, t)$, on the same assumption that $p(C, t)$ is equal to $p(C|S, t) p(S, t)$ because C belongs to S , and $\sum_{C \in \text{Msh}(S)} p(C|S, t)$ is equal to 1 similarly to the assumption in **The Convenience of RESI for Dealing with Large Scale Land Crust** (S3 Text). Here denoting the universe, i.e., the whole given map, by S^U , $p(C)$ means $p(C/S^U)$. In this sense, $Hr(S, t)$ means the contribution of clusters in S to the entropy of S^U , divided by the rate of earthquakes in region S among all in S^U .

Thus, a large positive value of $Hr(S, t)$ means that $H(S^U, t)$ increases by a large value due to the occurrence of one earthquake in S , meaning that a single earthquake in S corresponds to a stronger influence on the process in Fig.1. The stronger influence occurs, for example, if the single earthquake forms a new cluster in S where earthquakes have been sparse as the upper part of state (b) or the new bridge in a seismic gap as in state (d). Therefore, if $Hr(S, t)$ is converging to its maximum value, it can be expected that the structure of clusters in S^U is in the transition to (e). This convergence should be observed as the saturation after the increase in $Hr(S, t)$. If the perturbation of $Hr(S, t)$ is observed after this saturation, it means the earthquakes on the bridge in the state (d) may push the structure of clusters to state (e) and also back to (d). Thus we expect to detect precursors of earthquake activation in region S on the increase in $Hr(S, t)$ in Eq.(2), followed by its saturation, or the perturbation due to the unstable bridge in Fig.1 (d).

In addition, $Hr(S, t)$ for region S can be computed as the average of $Hr(S_i, t)$ for all regions S_i in S as shown in S3 Text. This makes it possible to compute the value of RESI for region S^+ that is a union of smaller regions such as S_i conveniently by a linear computation.

The algorithm to obtain alarms of precursor candidates on RESI

RESI is obtained by the two steps in this section: in Step 1 below, the clusters of quaking meshes (square areas of 0.1 deg of latitude and longitude including the foci of earthquakes occurred over a cutoff frequency) in the target region S are generated, and in Step 2 the value of RESI i.e., $Hr(S, t)$ for S is computed. The saturation or the unstable perturbation (as state (d) in Fig.1 mentioned above) of $Hr(S, t)$, following its increase in the transition from state {(a) or (b)} to (c) in Fig.1, is taken as a precursor of the activation of earthquakes.

Here let us divide the target region S into meshes of size $(\Delta x, \Delta y)$ that are to be clustered in Step 1 above, where Δx and Δy are the widths in latitude and longitude respectively. x_L and y_L respectively represent the widths in latitude and longitude of region S , substantially wider than meshes of width Δx and Δy . $[t, t+t_L]$ is the time range for which $Hr(S)$ is computed setting t_L to 1 year or 1 month as shown later. In Step 1-2), the quaking meshes represented by $Msh(S)$ is defined as the set of meshes where a given θ_m or a larger number of earthquakes of magnitude M_θ or larger occurred in the period $[t, t+t_L]$. The cutoff magnitude M_θ is set to 2.0 as mentioned in **Data and its Availability**. θ_m is set to 1, to avoid taking meshes having only one earthquake that may be a noise captured by chance with a seismograph. $p(X, t)$ for region X or cluster X is computed as $quakes(X, t)/quakes(S^U, t)$ where $quakes(X, t)$ is the number of earthquakes in X greater than magnitude M_θ in period $[t, t+t_L]$, and S^U here means the background including all clusters. Let us hereafter represent a rectangular area (mesh, cell, or wider region) of four vertices (x, y) , (x', y) , (x, y') , (x', y') , by $(x, y)-(x', y')$.

The clustering function **make_clusters**(S, t) called in Step 1-3) runs as follows (see the supplementary S1 Text, [referring to 52-55](#) and S1 and S2 Figures for details). That is, each cluster $C_{x_0y_0}$ grows as a subset of $Msh(S)$ (initialized in Step 1-2), from a seed mesh $m_{x_0y_0}$ selected randomly from quaking meshes belonging to no cluster generated so far. $C_{x_0y_0}$ grows by absorbing meshes in the neighbors of meshes in $C_{x_0y_0}$ itself, which are in $Msh(S)$ but are not yet in any cluster. Adding the neighbors of mesh m_{xy} in $C_{x_0y_0}$, from members of $Msh(S)$ not yet belonging to any clusters generated so far, to $C_{x_0y_0}$ is called to extend m_{xy} . And, the meshes already extended are called ‘‘Extended.’’ This cycle of seeding and growing clusters is iterated until all meshes in $Msh(S)$ get covered by the generated clusters. Here, the representation of a cluster by $C_{x_0y_0}$ means it is represented by its starting seed mesh $m_{x_0y_0}$. And, $surround(m_{xy})$ below is the set of 8 meshes surrounding m_{xy} , i.e., $\{m_{x-\Delta x, y+\Delta y}, m_{x, y+\Delta y}, m_{x+\Delta x, y+\Delta y}, m_{x-\Delta x, y}, m_{x, y}, m_{x+\Delta x, y}, m_{x-\Delta x, y-\Delta y}, m_{x, y-\Delta y}, m_{x+\Delta x, y-\Delta y}\}$. See Figure 2 for an illustration of **make_clusters**(S, t).

(Step 1: obtain clusters of quaking meshes in the target region S for the period $[t, t+t_L]$)

- 1-1) Divide the target region S that is $(x_0, y_0)-(x_0+x_L, y_0+y_L)$ into meshes of a given size $(\Delta x, \Delta y)$.
- 1-2) For the period $[t, t+t_L]$, take $Msh(S)$, the set of quaking meshes in S .
- 1-3) Do **make_clusters**(S, t).

(Step 2: obtain RESI) RESI is obtained as $Hr(S, t)$ on equation (2). C is a cluster of meshes in S , and $p(C|S, t)$ denotes the conditional probability that an earthquake occurred in C under the condition that its location was in region S , during the period $[t, t+t_L]$. $p(C|S, t)$ is the division of the number of earthquakes in C , by the number in region S , in $[t, t+t_L]$.

(Step 3: obtain the alarms of candidates of precursors) The time, when the value of $Hr_{sat}(S, t)$ defined below is larger than 0, i.e., when $Hr(S, t)$ saturates at the highest value range of the last period of length T , is taken as an alarm of the precursor of earthquake activation.

make_clusters(S, t)

Extended = {} (i.e., empty set);

while Msh(S) \neq {}:

m_{x0y0} := a randomly selected member of Msh(S); $C_{x0y0} = \{m_{x0y0}\}$

For each mesh m_{xy} in $C_{x0y0} \setminus \text{Extended}$: *#each mesh not extended yet gets extended below*

while Msh(S) \cap surround(m_{xy}) \neq {}

add_to_cluster = Msh(S) \cap surround(m_{xy})

$C_{x0y0} = C_{x0y0} \cup \text{add_to_cluster}$

Msh(S) = Msh(S) \setminus add_to_cluster

Extended = Extended + m_{xy}

Return

As mentioned already, we regard the precursor of a large earthquake in the state of Fig. 1 (e), as the convergence to the end of (c) or events in (d) that are respectively observed as the saturation or the perturbation after the saturation, of $\text{Hr}(S, t)$ i.e., RESI value. This is shown in Eq. (3), where $\text{Hr}_{\text{sat}}(S, t)$ larger than 0 means an alarm of the time we hypothesize as a precursor, according to the model since Fig.1.

$\text{Hr}_{\text{sat}}(S, t)$: return alarm below

if rank τ in $[t - \min(T, t), t]$ $\text{Hr}_{\text{avr}}(S, \tau = t) \leq \gamma \min(T, t)$ and

stdev τ in $[t - dt, t]$ $\text{Hr}(S, \tau) < \theta_{\text{std}}$

or stdev τ in $[t - dt/2, t]$ $\text{Hr}(S, \tau) > 2 \text{ stdev } \tau$ in $[t - dt, t - dt/2]$ $\text{Hr}(S, \tau)$

alarm = $\text{Hr}(S, t)$

else

alarm = 0

(3)

Here, $\text{Hr}_{\text{avr}}(S, t)$ is the average of $\text{Hr}(S, t)$ for the preceding 6 months $[t - 5, t]$. The first and the second lines respectively mean the top-ranked values of $\text{Hr}_{\text{avr}}(S, t)$ at time t in the last $\min(T, t)$ years where T is given, and the reduction of temporal variation of $\text{Hr}(S, t)$ due to its saturation in (c) of Fig.1. The third line means the perturbation of $\text{Hr}(S, t)$ during the transition period from (d) to (e) in Fig.1. dt is set to 1 year. In the case t_L is set to 1 year, $\text{Hr}_{\text{avr}}(S, t)$ is replaced with $\text{Hr}(S, t)$, and $\text{stdev } \tau$ in $[t - dt, t]$ ($\text{Hr}(S, \tau)$) with $|\text{Hr}(S, t) - \text{Hr}(S, t-1 \text{ year})|$ because only two data points are in $[t-1 \text{ year}, t]$. θ_{std} is set to 0.5, γ to 0.1 in the experiments below.

Results

We used data on the 0.61×10^6 earthquakes in Japan from 1983 through 2017 (see Data Availability, S4 Figure, and S1 Table), of the cutoff M_θ set to 2.0 or equal or larger. Regions dealt with in the remainder are in the square of (25,125)-(49,149) as shown in Fig 2, including the major portion of islands in Japan, where seismographs used for collecting the data above are located. This square has been divided into 36 cells, each corresponding to the region S above, of 4 deg in latitude and longitude i.e., nearly 450km square. For example, the left bottom cell is (25,125)-(29,129).

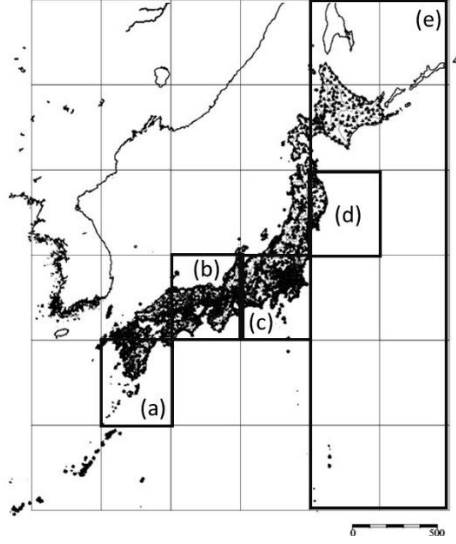


Figure 2. Division of (25,125)-(49,149) into 36 regions. The proposed method is evaluated for regions (a) through (f) in this figure. The small dots in the land area represent locations of seismographs. Source of the background map: Japan Meteorological Agency website (<http://www.data.jma.go.jp/svd/eqev/data/intens-st/>). The modification and the use of this map are licensed as in <http://www.jma.go.jp/jma/en/copyright.html>.

The error of epicenter location is suspected to be in the order of 10km as in the literature⁵⁶, that is close to 0.1 [deg] in latitude and longitude. According to the author's analysis, the average for all the years in the period of the available JMA catalog, of the average error of epicenters is $(1.19, 1.59) \times 10^{-2}$ [deg] and of the standard deviation is $(1.13, 1.71) \times 10^{-2}$ [deg] for (latitude X, longitude Y). Hence the mesh size of 0.1 deg square the finest in the range to absorb the errors of epicenters, i.e., larger than the average by 3 times of the standard deviation.

The time series of clusters and RESI

Here, let us show running examples of computing RESI. (x_L, y_L) is set to (4, 4) [deg] for dealing with regions (a) through (d) in Figure 2, and (24, 8) [deg] for (e) that includes region (d). t_L is set to 1 year or 1 month in the experiments, $(\Delta x, \Delta y)$ to (0.1, 0.1) [deg] as mentioned above. In Step 1 above, clusters of quaking meshes are obtained as colored in Fig. 3. Then in Step 2, $Hr(S, t)$ is obtained for each panel of (a) through (e) in Fig. 4 and Fig. 5, corresponding to each region of (a) through (e) in Fig. 3. Here RESI is roughly found to increase and then saturate a few years before activity(S, t) in equation (4) increases toward peaks. Eq.(4) represents the magnitude corresponding to the total energy of all earthquakes, $N_{t,S}$ the number of earthquakes, and $M_{t,S,k}$ the magnitude of the k -th earthquake, respectively in region S in the time unit $[t, t+t_L]$. 31.62 is the logarithm bottom for the JMA magnitude.

$$\text{activity}(S, t) = \log_{31.62} \sum_{k=1}^{N_{t,S}} 31.62^{M_{t,S,k}}. \quad (4)$$

In Figure 3 (a) through (e), let us see the clusters obtained in Step 1 and the alarms of precursors obtained on Eq.(3) for the five regions in the thick frames of Fig.2 (a) through (e). Then find the correlation of $Hr(S, t)$, $Hr_{\text{sat}}(S, t)$, and activity(S, t), setting t_L to 1 year in Figure 4 and 1 month in Figure 5, where panels (a) through (e) correspond to (a) through (e) in Figures 2 and 3 as follows.

- (a) In the change from 1993 to 1995 in the regions of Fig. 2 (a), new clusters emerge till 1994, corresponding to the increase in $Hr(S, t)$ in Fig. 4(a) and Fig. 5(a) till 1994. This increase saturated at (a-2) in 1995, before the earthquake of M6.9 in October 1996 at (a-1) in both Fig.4 and Fig.5. Thus, the target region itself came

to form the state of Fig.1 (c) or (d), followed by (d) and (e) of a large earthquake.

- (b) In the region of Fig. 2 (b), we find the increase of clusters till 2000, when RESI saturated as in Fig. 4(b) and Fig. 5(b). These clusters are located far, according to Fig.3 (b), from the focus of the M7.3 earthquake at (b-1) in Fig.4 and 5 in October 2000 marked by the red cross in Fig.3 (b). However, as in S5 Figure, the area of intense quaking due to this earthquake ranged in the areas of the clusters in Fig.3(b). The alarm of (b-2), obtained as the time of non-zero $Hr_{sat}(S, t)$, preceded (b-1) by one year in both Fig.4 and Fig.5.
- (c) In Fig. 3 (c), we find the increase in clusters till 1999, the time of the saturation at (c-2) of RESI in Fig. 4(c) and Fig. 5(c). Then, the earthquake of M6.1 at the red cross in Fig.3(c) occurred in August 2000, which reduced RESI substantially, as in (c-1) in both Fig. 4(c) and Fig. 5(c).
- (d) In the wide region (e) including region (d), as in Fig.3 (e) including (d), we find at least two clusters in the ocean have got united in 2011, one that existed since before 2006, the other where earthquakes increased since then. The main shock of M9.0 occurred on March 11th 2011 at the red cross between these clusters, then the clusters have got united. In Fig.4 (d), however, we find no precursory saturation for the earthquake of M9.0 at (d-1). On the other hand, we find the saturation of RESI at (e-2) in Fig. 4(e), where (e-1) represents the M9.0. In Fig.5 also, we find the precursor (e-2) for (e-1), but (d-2) is not so close to (d-1). These results will be discussed in the Discussion section.

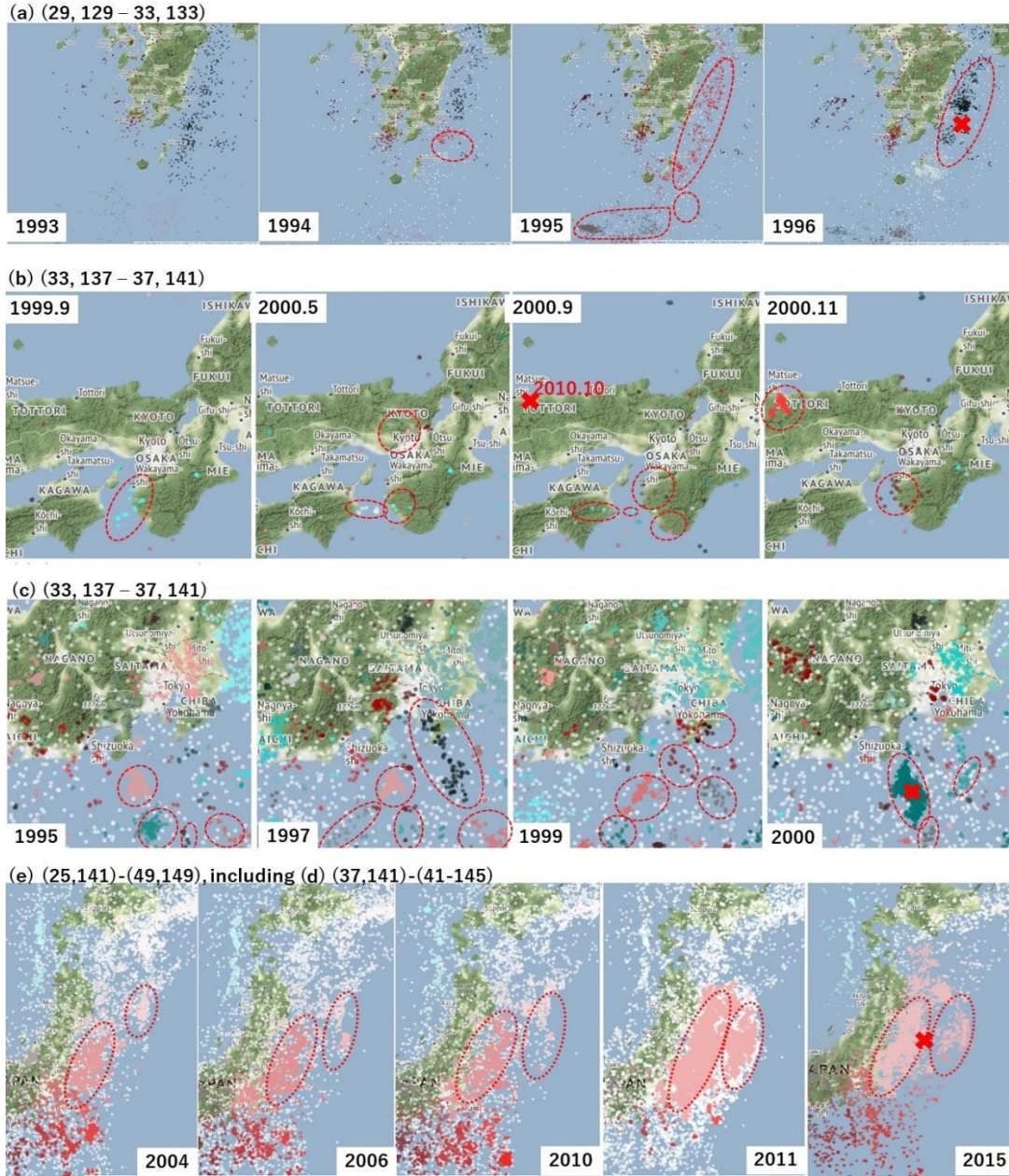


Figure 3. Running examples of Step (1): clusters obtained. The colors in (a) through (e) show clusters of quaking meshes obtained in Step 1, for the regions of Fig.2 (a) through (e). The red crosses show the epicenters of large earthquakes corresponding to the peaks of activity in Fig.4 and Fig.5. The dotted ellipses show clusters referred to in the text. The maps have been created using Folium copyrighted since 2013 by Rob Story, licensed under the MIT License (<https://github.com/python-visualization/folium/blob/master/LICENSE.txt>).

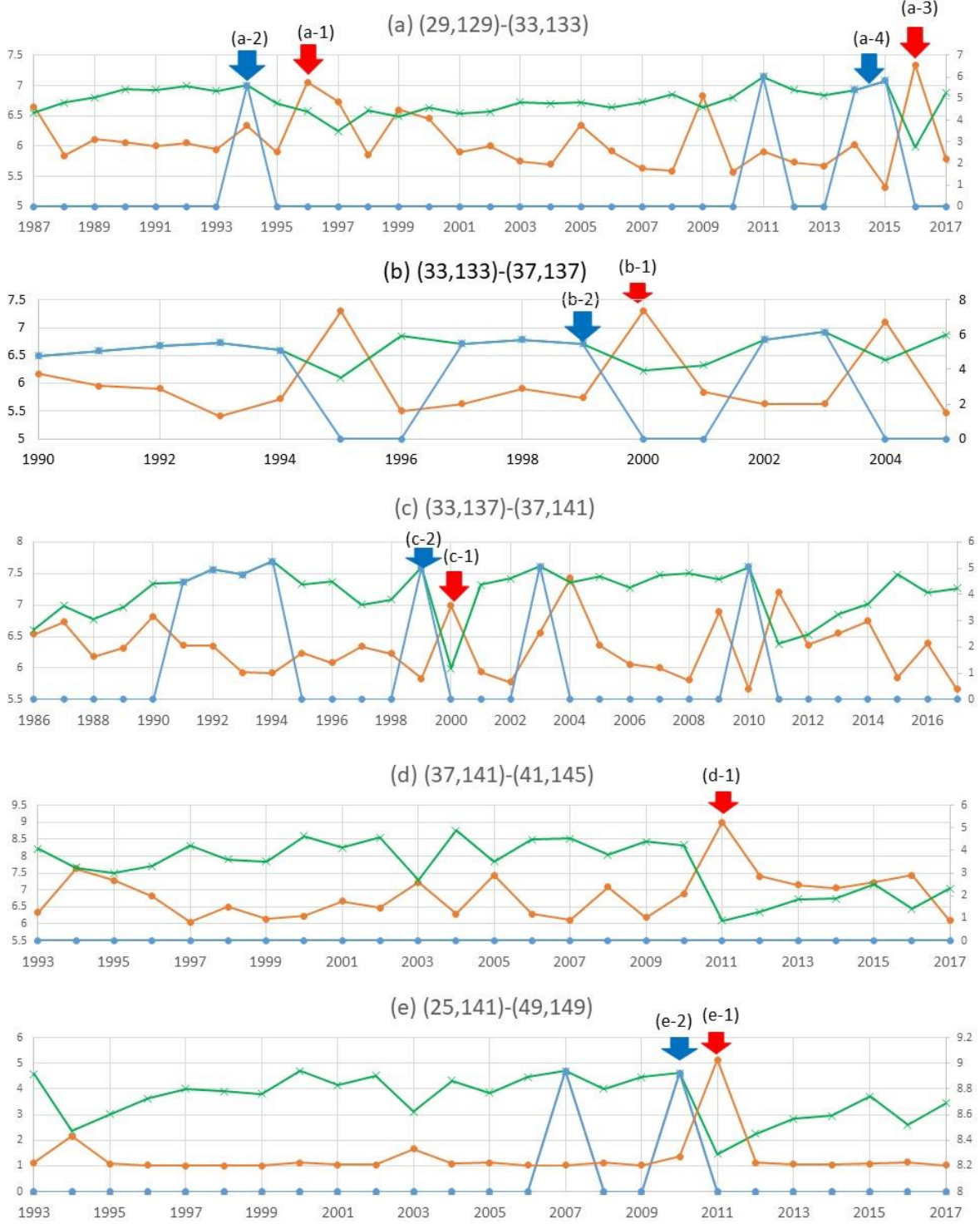


Figure 4. Running examples of Step (2) for t_L set to 1 year: RESI ($Hr(S, t)$, green line), the alarm of precursor obtained as Hr_{sat} on Eq.(3) (blue line), and the earthquake activity (orange) of each region. Panels (a) through (e) correspond to the five regions in Fig.3. (a-3) and (a-4) are referred to in the later Section than other arrows.

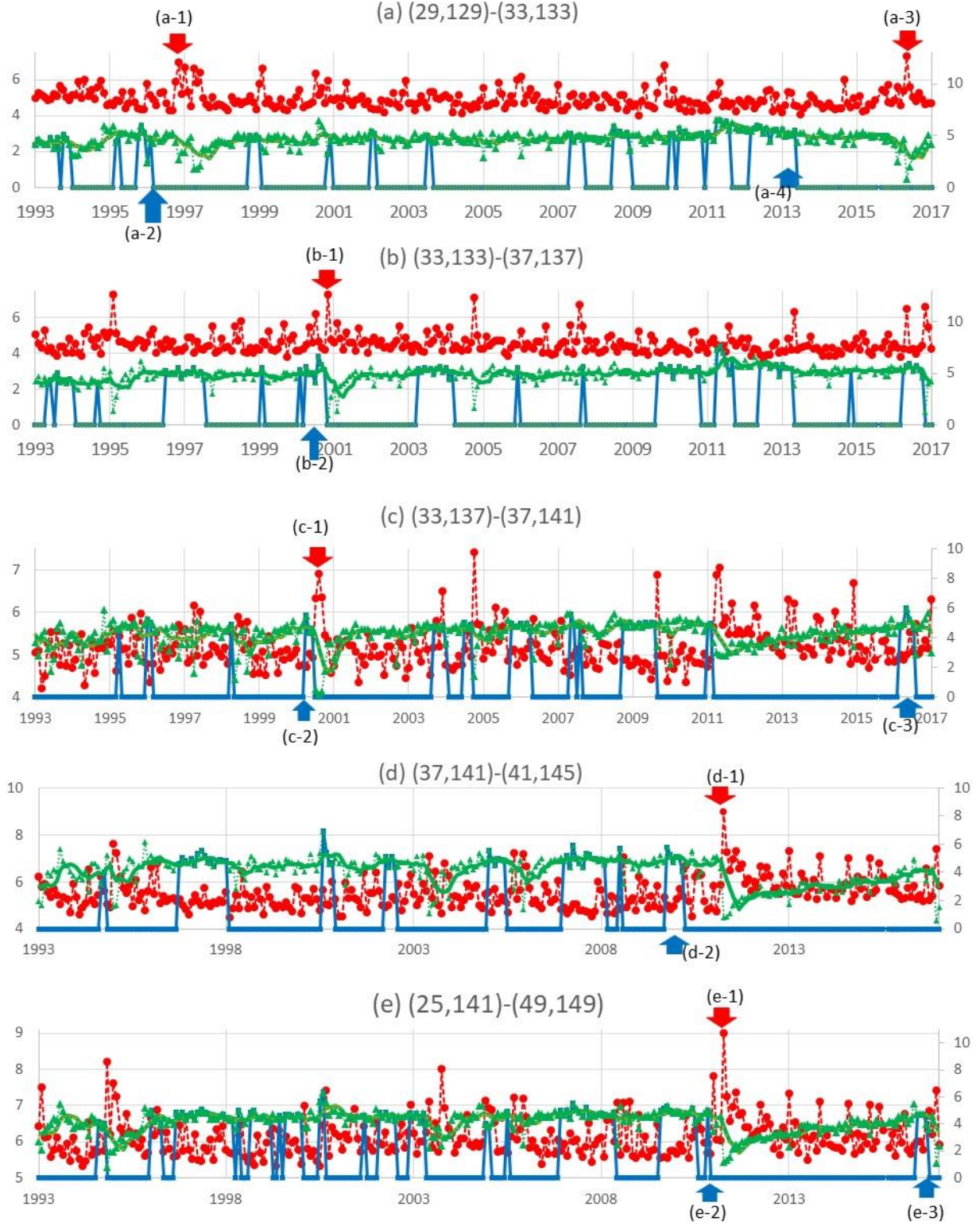


Figure 5. Running examples of Step (2) for t_L set to 1 month: setting other conditions same as Figure 4. (a-3), (a-4), (c-3), and (e-3) are referred to in the later Section than other arrows.

Measures for the Utility of RESI

Let us compare the utility of $\text{Hr}_{\text{sat}}(S, t)$ with baseline alarming methods, by computing its correlation (with delay or precedence) with $\text{activity}(S, t)$ for each region S that is a cell of 4 deg in latitude and longitude in Fig. 2. In this Section, for evaluating the precedence or the delay by a shorter time than a year, we set t_L to 1 month. In preparation, let us define meta-function high_f for function f for each region S as follows. For Hr as f ,

$$\begin{aligned} \text{if } \text{Hr}_{\text{sat}}(S, t) > 0: & \quad \text{high_Hr}(S, t) = 1 \\ \text{else:} & \quad \text{high_Hr}(S, t) = 0 \end{aligned} \quad (5)$$

Then, if f is a baseline function to be compared with RESI, that may be PI or RI summarized in Supplementary S4 Text [referring to 30 - 39](#), $\text{high}_f(S, t)$ is set to 1 for t 's of the largest n values of $f(S, t)$, where n is equal to $m T_f / T_{\text{Hr}}$ for m , the number of all t where $\text{Hr}_{\text{sat}}(S, t) > 0$, in order to make a fair comparison with RESI. Here, T_{Hr} is the length of the time where Hr is defined and T_f is the length of the period where f is defined (i.e., where $t > t_1$ and $t > t_0$ for PI and RI as shown in S4 Text, and $t > \text{Jan 1986}$ for RESI cutting the first 3 years as noise in Eq.(3) because T larger than 3 years did not affect the performance of the alarm as mentioned later in **Discussions** on S8 Fig). On the other hand, about the earthquake activity, that is not a baseline to compare with RESI but the target to predict, $\text{high_activity}(S, t)$ is set to 1 if $\text{activity}(S, t)$ at time t is larger than its average plus the standard deviation for all the data period and is the largest in the time range of $[t-2 \text{ years}, t]$. Thus, months of significantly larger total magnitude of earthquakes than average, without an earthquake of equal or larger magnitude within 2 preceding years, are taken.

Then, on equations (6) through (8), $\text{prec}(f, g, S, \Delta t)$ and $\text{delay}(f, g, S, \Delta t)$ respectively mean the probability that the high value of $f(S, t)$ appeared earlier and later than $g(S, t)$ within a time gap of Δt . Thus, $\text{prec}(f, g, S, \Delta t)$ and $\text{delay}(g, f, S, \Delta t)$, defined in equations (7) and (8) respectively, both imply the possibility to regard f as a precursor of g . However, the utility of the two functions are different: $\text{prec}(f, \text{activation}, S, \Delta t)$ suggests to expect the activation of earthquakes in the following period of Δt if an alarm defined on f is detected at t , whereas $\text{delay}(\text{activation}, f, S, \Delta t)$ suggests looking back at an alarm in the past Δt months, if activation is detected at t . Δt is set to 1, 2, or 3 years in the following tests. Details of the reason for choosing the evaluation method above are in the Method for Evaluating Alarming Functions, referring to the literature^{15, 16, 57-59} in S5 Text.

$$\text{unit}(x) = 1 \text{ if } x > 0, \text{ unit}(x) = 0 \text{ if } x = 0 \quad (6)$$

$$\text{prec}(f, g, S, \Delta t) = \frac{\sum_{t=ts}^{te-\Delta t} \text{unit}(\text{high}_f(S, t) \sum_{\tau=1}^{\Delta t} \text{high}_g(S, t+\tau))}{\sum_{t=ts}^{te-\Delta t} \text{unit}(\text{high}_f(S, t))} \quad (7)$$

$$\text{delay}(g, f, S, \Delta t) = \frac{\sum_{t=ts+\Delta}^{te} \text{unit}(\text{high}_g(S, t) \sum_{\tau=1}^{\Delta t} \text{high}_f(S, t-\tau))}{\sum_{t=ts+\Delta}^{te} \text{unit}(\text{high}_g(S, t))} \quad (8)$$

Comparison with baselines

In the evaluation, the values of $\text{prec}(f, g, S, \Delta t)$ and $\text{delay}(g, f, S, \Delta t)$ are computed, substituting g and f respectively with $\text{activity}(S, t)$ and the alarming function that is $\text{Hr}_{\text{sat}}(S, t)$, $\text{PI}(S, t_0, t_1, t)$, or $\text{RI}(S, t_0, t_1, t)$. $\text{PI}(S, t_0, t_1, t)$ represents the estimated risk of earthquakes in region S , represented by $\Delta \text{Pi}(t_0, t_1, t)$ in the reference of pattern informatics (PI^{30, 31, 34-38}). On the other hand, RI stands for the relative intensity (RI^{34, 36, 39}). PI and RI are summarized in the **S4 Text (Outlines of Compared Baselines** [referring to 30, 31, 34, 38, 39](#)). Then, the following evaluation is executed. Here $\text{random}(S, t)$ is a function to take 1 for all t , that means to present an alarm of precursor at a time chosen randomly. Function f is regarded as a precursor of g , that peaks earlier than g within the preceding time of Δt , if $\text{prec}(f, g, S, \Delta t) > \text{prec}(\text{random}, g, S, \Delta t)$. On the other hand, function g is regarded as an offshoot of f , or f is regarded as a precursor of g for a retrospect from g if $\text{delay}(g, f, S, \Delta t) > \text{delay}(g, \text{random}, S, \Delta t)$. In summary, the alarming functions are compared as in the following procedure.

The evaluation of the performance (Conditions A and B are two types of successful alarms)

for each alarming function in $\{Hr_{sat}, PI, RI\}$ **do**

$f = \text{alarming_function}$

if $\text{prec}(f, \text{activity}, S, \Delta t) > \text{prec}(\text{random}, \text{activity}, S, \Delta t)$: /* Condition A

f detects a precursor as an alarm of earthquake activity in region S within advance time Δt

if $\text{delay}(\text{activity}, f, S, \Delta t) > \text{delay}(\text{activity}, \text{random}, S, \Delta t)$: /* Condition B

f detects a precursor for a retrospect from earthquake activity in region S within time Δt

end if

end for

The performance of f as an alarming function of earthquake activation is evaluated as in Fig.6, on the values of prec and delay with visual representation. This evaluation has been executed for the 36 regions in Fig. 2, setting Δt to 12, 24, or 36 months, i.e., 1, 2, 3 years, for $\text{prec}(f, g, S, \Delta t)$ and $\text{delay}(g, f, S, \Delta t)$. Here it should be noted that the average temporal distance between successive times of non-zero $\text{high_activity}(S, t)$, i.e., δt where $t + \delta t$ is the nearest time after t where $\text{high_activity}(S, t) > 0$ and $\text{high_activity}(S, t + \delta t) > 0$, was 59.3 months and the standard deviation σ is 7.61, averaging for all the 22 cells where the monthly average number of earthquakes of M2.0 or larger was 1 or larger. That is, the evaluation comes to be meaningless if Δt is set longer than 36 months because $(\delta t - \Delta t)$ comes to be less than 3σ so it becomes unclear if the alarm was relevant to a future earthquake as a precursor or to a previous earthquake via some causality. This is the reason why we do not include results for Δt longer than 3 years.

Other indices, such as the changing of topic distribution on the dynamic topic models (DTM ⁶⁰) that can be applied to a sequence of discretized events, may be introduced in the future for the detection of changing points in earthquake history if extended to involve new topics corresponding to new latent dynamics which may cause earthquake precursors. However, DTM is not compared with RESI here, because RESI i.e., $Hr(S, t)$, itself is a function representing the distribution of events to clusters corresponding to events caused by latent topics in DTM. That is, RESI and DTMs are tools to be combined, rather than compared.

Discussions

The curves in Fig. 4 and 5 provide an intuition that the peaks of RESI precede the peaks of earthquake activity. As already mentioned, we find the saturation of RESI at (e-2) in Fig. 4(e), where (e-1) represents the M9.0 earthquake, whereas we do not find such a precursor in Fig.4 (d). A similar tendency was found in Fig.5. Considering the wide frame (e) in Fig.2 covers not only the red cross in Fig.3 (e) but also the epicenters of all the earthquakes larger than M7.0 within an hour after the main shock of M9.0 ⁶¹, which region (d) did not cover, these results are interpreted that the great earthquake occurred from the dynamics of a wider area than a cell in Fig.2. This example shows we should choose a suitable land scale for evaluating risks on RESI.

Some failures are found in the results, e.g., (a-3) does not appear within a few years after (a-4) in Fig.5, as does in Fig.4. Such a difference occurs because of the difference in the computation method for t_L set to 1 month and to 1 year in this paper as state below Eq.(3), so we should say the choice of t_L may affect the result. The change in $Hr(S, t)$ is the less stable for the shorter t_L because the number of events is the smaller in the period $[t, t_L]$, that is compensated by taking the average as $Hr_{avr}(S, t)$. However, in Fig.5, we find here the decrease in Hr for the

three years after (a-4) before a large earthquake at (a-3), that is an exceptional phenomenon – H_r usually tends to increase in the long time scale as in S7 Fig. Also, some panels include peaks of $H_{r\text{sat}}(S, t)$ such as Fig.5 (c-3) and (e-3) without any following peaks of earthquake activity. This does not always mean there is no risk, but may imply the possibility of a forthcoming large earthquake in the region. In Hokkaido, that is the north island in region (e) but not in (d), we really had M6.7 earthquake in September 2018, within 2 years from (e-3).

Figure 6 (a), (b), (c), and (d) show the preceding correlation of alarming functions with activity(S, t), for the evaluated period (data from 1983 to March 2017). Here, as in the red dots in the cells, that means Conditions A or B are satisfied respectively, we find the correspondence of these regions, with the 22 shadowed cells where the monthly average number of earthquakes of M2.0 or larger is 1 or larger. Note these shadowed cells correspond to regions where seismographs managed by JMA are located. That is, RESI substantially outperformed PI and RI for the tested precedence (i.e., advance) time Δt of 1 and 2 years. For Δt of 3 years or longer, less meaningful than Δt of 1 and 2 years as stated above, the difference in performance is not obvious.

About $H_{r\text{sat}}(S, t)$, T in Eq.(3) is here ideally set to 28 years, because the value of $H_{r\text{sat}}(S, t)$ tends to increase monotonously for at least 28 years as in S7 Figure. However, as shown in S8 Figure, the results are similar for any T from 3 to the larger value for the correlation for Δt of one year. For the longer precedence, such as 3 years for Δt , the figure shows the performance degrades for the shorter T . The superiority of RESI is expectable for Δt of 1 or 2 years, i.e., RESI detects precursors by the finest time resolution of a short period.

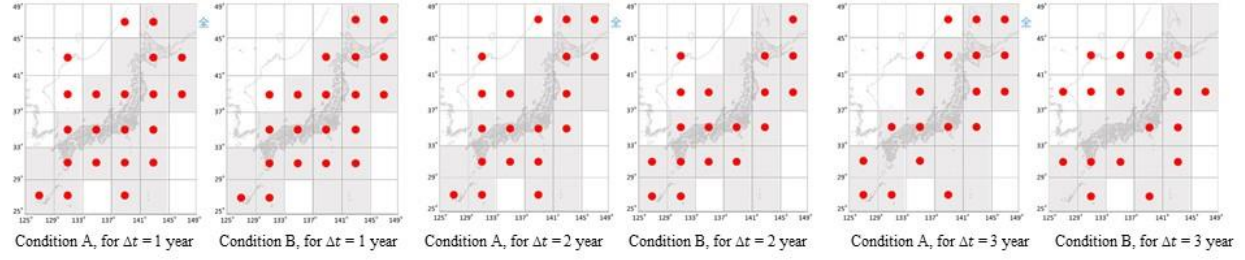
Conclusions

Based on the model of restructuring clusters of quaking meshes, we developed a method to detect precursors of earthquake activation in region S on the increase in RESI, that means the average contribution per earthquake in the target region to the diversity of clusters in the whole map. The alarm of precursor is detected when the increase in RESI is followed by its saturation or the perturbation after the saturation. As a result, RESI substantially outperformed PI and RI for the tested precedence (i.e., advance) time Δt of 1 and 2 years, i.e., RESI detects precursors by the finest time resolution of a short period.

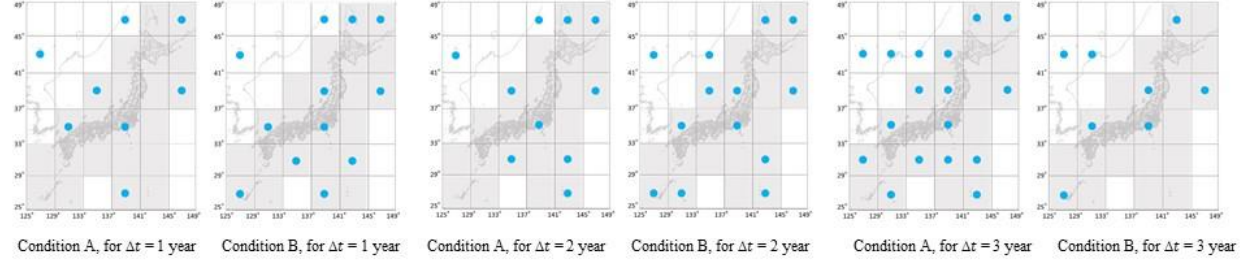
We should note that a change in the value of RESI may not only mean transitions of (a), (b), (c), (d), or (e) in Fig. 1, but may imply some mixture of them. Analysts are recommended to investigate further for investigating real latent dynamics if one detects a saturation of $H_r(S, t)$ at a high value, by expanding the data scale as from Fig. 2 (d) to (e) or collecting additional information such as data from sensing devices^{62, 63}.

Acknowledgements: This work was supported by JST CREST Grant Number JPMJCR1304, JSPS KAKENHI JP16H01836, and JP16K12428.

RESI



PI



RI

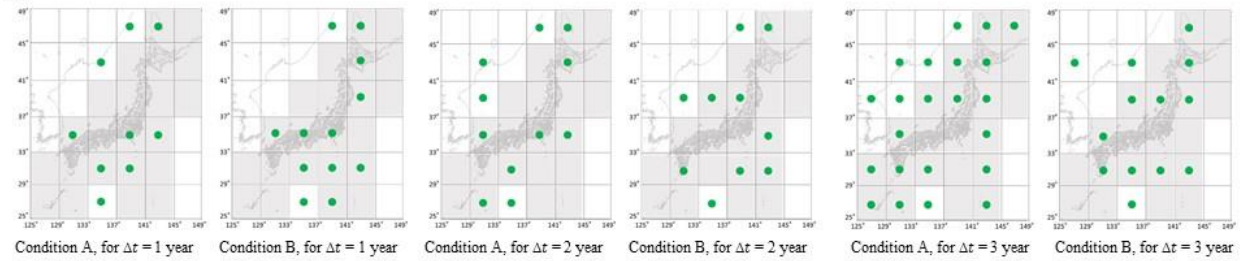


Figure 6. The performance of the compared alarming functions. Alarming functions $Hr(S, t)$, $PI(S, t)$, $RI(S, t)$ are compared for setting Δt to 1, 2, and 3 years respectively in (a), (b), and (c) here. The red dots in a cell mean Condition A stands in the left panel, and Condition B in the right, for each alarming function and for each value of Δt . The shadowed cells show regions where Source of the background map: Japan Meteorological Agency website (<http://www.data.jma.go.jp/svd/eqev/data/intens-st/>)

Data and their Availability

The target data are taken from the open catalog (S4 Figure) provided by Japan Meteorological Agency, including the time, latitude, longitude, magnitude, etc. These data can be downloaded from the open data site of Japan Meteorological Agency (<http://www.data.jma.go.jp/svd/eqev/data/bulletin/hypo.html>). This is the Japanese version of the one of English https://www.data.jma.go.jp/svd/eqev/data/bulletin/shindo_e.html, but the data of 2017 (till April) is added to the Japanese page. In addition, the location of seismographs is obtained by the same agency at <http://www.data.jma.go.jp/svd/eqev/data/intens-st/>, as visualized in Fig.2.

We cut off earthquakes below M_0 set to 2.0, that is a smaller cutoff than usual, e.g., 3.0 as in the literature [32, 35, 64](#) etc, and obtained all earthquakes in the data from 1983 till March 2017, as shown in Table S1. The reason for taking such a small cutoff is because RESI stands on the distribution of earthquakes, of which small ones occupy a large portion, in addition to the purpose to use the data of aftershocks as mentioned in **Dealing with Small Earthquakes (S2 Text)**.

The values of magnitude and focal positions have been collected in a different regulation before and after 1983 ^{65,66}, so we have not used data of earthquakes before 1983. Although the clustering of quaking meshes can be extended easily to 3-dimensional data, here two dimensions, i.e., latitude and longitude, are dealt because earthquakes of low energy are analyzed due to the low cutoff value M_θ as stated already, for which the information about the depth is not as reliable as for larger earthquakes.

References

1. Scholz, C. H. *The mechanics of earthquakes & faulting*, 2nd edition (Cambridge University Press, 2002).
2. Gabrielov, A., Zaliapin, I., Newman, W.I. & Kelis-Borok, V.I. Colliding cascades model for earthquake prediction, *Geophys. J. Int.* **143**, pp.427-437 (2000).
3. Turcotte, D. L. Earthquake prediction, *An. Rev. Earth Planet. Sci.* **19**, 263-281 (1991).
4. Lomnitz, C. *Fundamentals of earthquake prediction* (John Wiley, New York, 1994).
5. Kelis-Borok, V. Earthquake predictions: state-of-the-art and emerging possibilities, *An. Rev. Earth Planet. Sci.* **30**, 1-33 (2002).
6. Kanamori, H. Earthquake prediction: an overview, in Lee, W. H. K., Kanamori, H., Jennings, P. C. , Kisslinger C. (eds.) *International Handbook of Earthquake & Engineering Seismology*, 1205-1216. (Academic Press, Amsterdam, 2003).
7. Gonzalez-Ruiz, J.R. & McNarilly, K.C. Stress accumulation and release since 1882 in Ometepe, Guerrero, Mexico: implications for failure mechanisms and risk assessments of a seismic gap, *J. Geophys. Res.*, **93**(B6), 6297-6317 (1988)
8. Dobrovolsky, I. P., Zubkov, S. I. & Miachkin, V. I. Estimation of the size of earthquake preparation zones, *Pure Appl. Geophys.* **117**, 1025-1044 (1979).
9. Press, F. & Allen, C. Patterns of seismic release in the southern California region, *J. Geophysics Research* **100**, 6421-6430 (1995).
10. Lee, J.A., Mining quantitative association rule of earthquake data, *Proc. Int'l Conf. Convergence and Hybrid Information Technology*, 349-352 (2009).
11. Lei, L., Identify Earthquake hotspots with 3-dimensional density-based clustering analysis, *Proc. IEEE Int'l Geoscience and Remote Sensing Symp.* pp.530-533 (2010).
12. Ansari, A., Noorzad, A., & Zafarani, H. Clustering analysis of the seismic catalog of Iran, *J. Computers & Geosciences* **35** (3) 475-486 (2009).
13. Fukui, K., Inaba, D. & Numao, M. Discovering seismic interactions after the 2011 Tohoku earthquake by co-occurring cluster mining, *Information and Media Technologies* **9** (4), 886-895 (2014).
14. Fearnhead, P. & Liu, Z. Online inference for multiple changepoint problems. *J. Royal Statistical Soc.: Series B* **69** (4), 589-605 (2007).
15. Hayashi, Y. & Yamanishi, K. Sequential network change detection with its applications to ad impact relation analysis, *Data Mining and Knowledge Discovery* **29**, 137-167 (2015).
16. Miyaguchi, K., & Yamanishi, K. Online detection of continuous changes in stochastic processes *Int'l J. Data Science and Analytics* **3**(3) , 213-229 (2017)
17. Smolka, A., The earthquakes of Northridge 1994 and Kobe 1995 – lessons for risk assessment and loss prevention with special reference to earthquake insurance, *The 11th World Conf. on Earthquake Engineering* paper no. 1947 (1996)
18. Normile, D. Devastating earthquake defied expectations, *Science* **331**, 6023, 1375-1376 (2011)
19. Chandle, D. MIT shows China quake was rare event, could be a long wait before next big temblor--or maybe not, *MIT News Office* June 30, 2008, <http://news.mit.edu/2008/quake-china-0630>
20. Charola, A.E., Wegener, C., & Koestler, R.J. (eds) Unexpected - earthquake 2011: lessons to be learned, *Smithsonian Contributions to Museum Conservation* (2014)

21. Martínez-Álvarez, F., Troncoso, A., Morales-Esteban, A. & Riquelme, J.C., Computational intelligence technologies for predicting earthquakes, *LNAI* **6679** (2), 287-294 (2011).
22. Kagan, Y.Y., & Jackson, D.D. Probabilistic forecasting of earthquakes, *Geophys. J. Int.* **143**, 438-453 (2000).
23. Ogata, Y. & Zhang, J. Space-time ETAS models and an improved extension, *Technophysics* **413**, 13-23 (2006).
24. Zhuang, J., Long-term earthquake forecasts based on the epidemic-type aftershock sequence (ETAS) model for short-term clustering, *Research in Geophysics* volume 2:e8 pp.52-57 (2012)
25. Sornette, D. & Sammis, C. Complex critical exponents from renormalization group theory of earthquakes: implications for earthquake predictions, *J. Physique-I* **5**, 607-619 (1995).
26. Keilis-Borok, V. I., Knopoff, L. & Rotvain, I.M. Bursts of aftershocks, long-term precursors of strong earthquakes, *Nature* **283**, 259-263 (1980).
27. Keilis-Borok, V.I., The lithosphere of the earth as a nonlinear system with implications for earthquake prediction, *Rev. Geophys.* **28** (1), 19-34 (1990).
28. Keilis-Borok, V. I., Intermediate-term earthquake prediction, *Proc. Natl. Acad. Sci.* **93**, 3748-3755 (1996).
29. Keilis-Borok VI, Rotvain IM. 1990. Diagnosis of time of increased probability of strong earthquakes in different regions of the world: algorithm CN. *Phys. Earth Planet. Inter.* 61: 57-72
30. Nanjo, K.Z., Rundle, J.B., Holliday, J.R. & Turcotte, D.L. Pattern informatics and its application for optimal forecasting of large earthquakes in Japan, *Pure Appl. Geophys.* **163**, 2417-2432 (2006).
31. Nanjo, K.Z., Holliday, J.R., Chen, C.-c., Rundle, J.B. & Turcotte, D.L. Application of a modified pattern informatics method to forecasting the locations of large future earthquakes in the central Japan, *Tectonophysics* **424**, 351-366 (2006).
32. Rundle, J. B. , Tiampo, K. F., Klein, W. & Martins, J. S. S. Self organization in leaky threshold systems: The influence of nearmean field dynamics and its implications for earthquakes, neurobiology, and forecasting, *Proc. Natl. Acad. Sci. USA* **99** (Suppl. 1), 2514-2521 (2002).
33. Rundle, J. B., Turcotte, D. L., Shcherbakov, R., Klein, W. & Sammis, C. Statistical physics approach to understanding the multiscale dynamics of earthquake fault systems, *Rev. Geophys.* **41**, 1019-1038 (2003).
34. Holliday, J.R., Nanjo, K.Z., Tiampo, K.F., Rundle, J.B. & Turcotte, D.L. Earthquake forecasting and its verification, *Nonlinear Processes in Geophys.* **12**, 965-977 (2005).
35. Tiampo, K.F., Rundle, J.B., Klein, W. & Holliday, J.R. Forecasting rupture dimension using the pattern informatics technique, *Tectonophysics* **424**, 367-376 (2006).
36. Rundle, J. B. *et al.* The 1999 Chi-Chi, Taiwan, earthquake as a typical example of seismic activation and quiescence, *Geophys. Res. Lett.* **32**, L22315 (2005).
37. Zhang, Y., Zhang, X., Yin, X., & Wu, Y. Study on the forecast effects of PI method to the north and southwest China, *Concurr. Comp-Pract. E.* **22**, 1559-1568 (2010).
38. Zhang, Y., Zhang, X., Wu, Y., & Yin, X., Retrospective study on the predictability of pattern informatics to the Wenchuan M8.0 and Yutian M7.3 earthquakes, *Pure Appl. Geophys.* **170** (1), 197-208 (2012).
39. Nanjo, K.Z. Earthquake forecast models for Italy based on the RI algorithm, *Ann. of Geophys.* **53** (3), 117-127 (2010).
40. William K. Mohanty, Alok K. Mohapatra, Akhilesh K. Verma, Kristy F. Tiampo & Kaushik Kislay (2016) Earthquake forecasting and its verification in northeast India, *Geomatics, Natural Hazards and Risk*, 7:1, 194-214,
41. Ohsawa, Y. KeyGraph as risk explorer from earthquake sequence, *J. of Contingencies and Crisis Management* **10** (3), 119-128 (2002).
42. Shannon, C.E., A mathematical theory of communication, *Bell System Technical Journal* **27**, 379-423 (1948)
43. Lieb, E. H.; Yngvason, J. (1999). "The Physics and mathematics of the second law of thermodynamics". *Phys. Rept.* 310: 1.
44. Koyama J., Motoya Y. & Hara, H. Complex activity of earthquakes characterize by the maximum entropy, *Geophys. Bulletin Hokkaido Univ.* **60**, 77-95 (1997)
45. Li, T., Ma, S., & Ogihara, M. Entropy based criterion in categorical clustering. *Int'l Conf. on Machine Learning*, 68-75 (2004)

46. Kahn, B.K., Consumer variety seeking among goods and service, *J. Retailing and Consumer Services* **2**, 139-148 (1995)
47. Alexander, P.J., Product variety and market structure: a new measure and a simple test, *J. Economic Behavior & Organization* **32** (2), 207-214 (1997)
48. Grigoriev, A.V., The evaluation of variety of market structure using the entropy indicator, *J. Siberian Federal University. Humanities & Social Sciences* **4**, 521-527 (2012)
49. Fuchs, M., Homann, R. & Schwonke, F. Comparison of images taken by different sensors, *Geinformatics FCE CTU* **3**, 28-28 (2008)
50. Nychis, G., Sekar, V., Andersen, D.G., Kim, H. & Zhang, H. An empirical evaluation of entropy-based traffic anomaly detection. *Proc. of the 8th ACM SIGCOMM Conf. Internet Measurement*, 151 – 156 (2008)
51. Winter, P., Lampesberger, H., Zeilinger, M., & Hermann, E.. On detecting abrupt changes in network entropy time series. *IFIP International Conference on Communications and Multimedia Security*, 194-205 (2011)
52. Aggarwal, C.C., and Reddy, C.K., *Data Clustering: Algorithms and Applications*. CRC Press (2013)
53. Ye, J., Zhao, Z. & Wu, M. Discriminative k-means for clustering. *Advances in Neural Information Processing Systems* **20**, 1649-1656 (2008)
54. Xie, J., Girshick, R. & Farhadi, A. Unsupervised deep embedding for clustering analysis, *Proc. of the 33 rd Int'l Conf. on Machine Learning*, 478-487 (2016)
55. Nie, F., Zeng, Z., Tsang, I. W., Xu, D., and Zhang, C. Spectral embedded clustering: a framework for in-sample and out-of-sample spectral clustering. *IEEE Trans. on Neural Networks* **22**(11) 1796–1808, 2011
56. Husen, S., and J.L. Hardebeck (2010), Earthquake location accuracy, Community Online Resource for Statistical Seismicity Analysis, doi:10.5078/corssa-55815573. Available at <http://www.corssa.org>.
57. Salvador, S. & Chan, P. FastDTW: Toward accurate dynamic time warping in linear time and space. *Proc. KDD WS on Mining Temporal and Sequential Data*, 70-80 (2004).
58. Nesaei, S., Sharafat, A.R., Real-time detection of precursors to epileptic seizures: non-linear analysis of system dynamics, *J. Medial Signals and Sensors* **4**(2), 103–112 (2014)
59. Melnyk, I., Yadav, P., Steinbach, M., Srivastava, J., Kumar, V. & Banerjee, A., Detection of precursors to aviation safety incidents due to human factors, *IEEE 13th International Conference on Data Mining Workshops*, 407-412 (2013)
60. Blei, D., Lafferty, J.D. Dynamic topic models, *Proc. Int'l Conf. on Machine Learning* **23**, 113-120 (2006)
61. Japan Meteorological Agency (JMA), The 2011 off the Pacific coast of Tohoku Earthquake Location of the Main Shock and Aftershocks https://www.jma.go.jp/jma/en/2011_Earthquake/chart/2011_Earthquake_Aftershocks.pdf (2011)
62. Loveless, J.P. & Meade, B.J. Geodetic imaging of plate motions, slip rates, and partitioning of deformation in Japan, *J. Geophys. Res.* **115**, B02410 (2010).
63. Wilson, J., Open source visualization of GPS displacements for earthquake cycle physics, *Google Research Blog* <https://research.googleblog.com/2016/11/open-source-visualization-of-gps.htm>
64. Frankel, A. F., Mapping seismic hazard in the central and eastern United States, *Seis. Res.Lett.* **60** (4), 8–21 (1995)
65. Hamada, N., Yoshida, A. & Hashimoto, H. Improvement of the hypocenter determination program of the Japan Meteorological Agency, *Quarterly Journal of Seismology* **48**, 35-55 (1983), in Japanese
66. Takeuchi, H. Magnitude determination of small shallow earthquakes with JSM electromagnetic seismograph model, *Quarterly Journal of Seismology* **47** pp.112-116 (1983), in Japanese

The Supplementary File for

“Regional Seismic Information Entropy for Detecting Precursors of Earthquake Activation”

Author list (single author): * Yukio Ohsawa

Affiliation of Author: Department of Systems Innovation, School of Engineering, The University of Tokyo (Japan), Postal address: 7-3-1 Hongo, Bunkyo-ku Tokyo 113-8656 Japan

***Correspondence** to [ohsawa@sys.t.u-tokyo.ac.jp]

Supplementary Texts: S1 – S5

- S1 Text: The clustering method in Step 1
- S2 Text: Dealing with Small Earthquakes
- S3 Text: The Convenience of Regional Entropy for Analysis
- S4 Text: The Outlines of Compared Baselines
- S5 Text: The Method for Evaluating Alarming Functions

Supplementary Figures and Table: S1 – S9

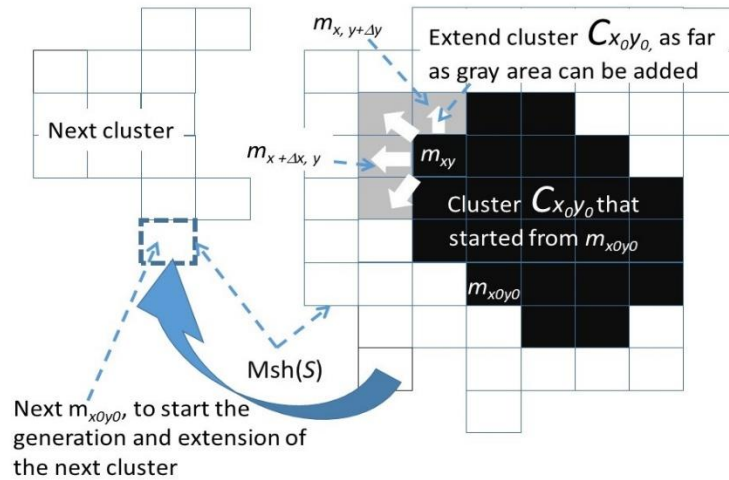
- S1 Figure: Clustering of quaking meshes in $Msh(S)$.
- S2 Figure: Clustering by $make_clusters(S, t)$ in Step 1, compared with k -means for various k 's, for imaginary regions
- S3 Figure: The reason why aftershocks should not be cut off here
- S4 Figure: The data structure in the earthquake catalog of JMA
- S5 Figure. The distribution of earthquake intensity
- S6 Figure. Computing $\langle \Delta I_i(t_0, t_1, t) \rangle$ in obtaining $PI(S_i, t_0, t_1, t)$ in Eq.(12)
- S7 Figure. The monthly transition of RESI for all regions and all Japan
- S8 Figure. The performance of the compared alarming functions
- S9 Figure. ROC/AUC, if applied, for an imaginary example
- S1 Table: The number of earthquakes of M2.0 or larger in the target

S1 Text: The clustering method in Step 1

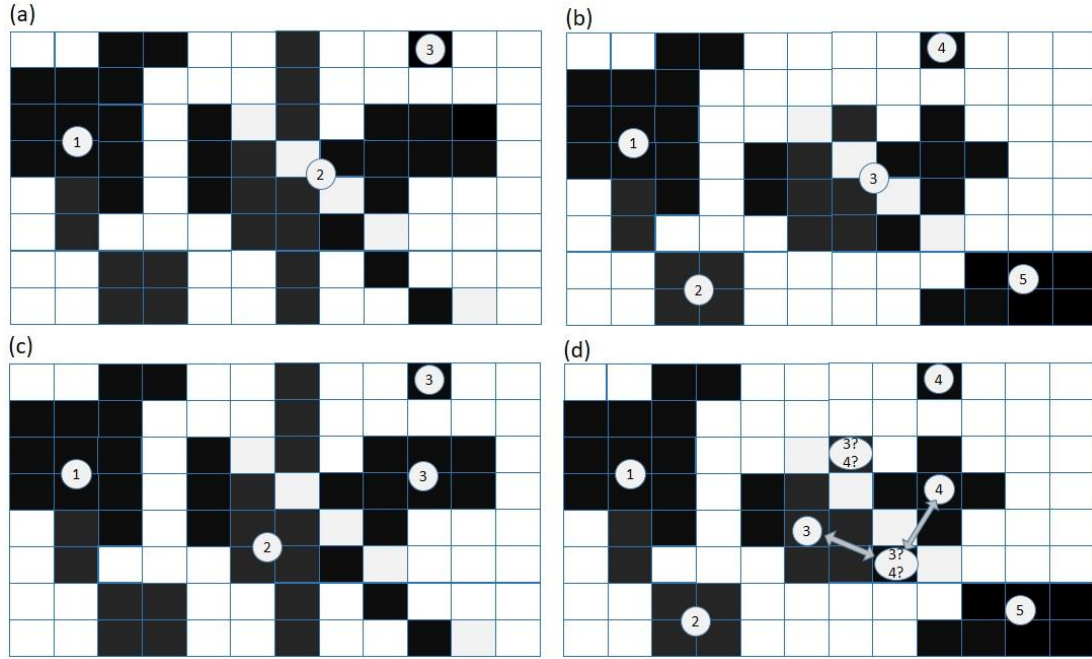
*Linked from the algorithm to obtain alarms of precursor candidates on RESI

The point of this paper is to detect precursors by computing regional entropy in Step 2, based on the distribution of earthquakes to clusters of quaking meshes obtained in Step 1. The method in Step 1 is introduced for the specific purpose to divide the land surface into such clusters separated by gaps composed of meshes where the frequency of earthquakes is low. The comparison with other methods for clustering^{52, 53} for a more general purpose is out of scope here. However, we can point out **make_clusters** called from Step 1 guarantees to run in time and memory of $O(n)$ for n as the number of all meshes in the map, meaning substantially lower cost than the up-to-date methods for unsupervised learning such as the unsupervised deep neural network⁵⁴.

More importantly, **make_clusters** fits the purpose to detect the changes corresponding to the transitions in Fig. 1. That is, the clustering here is required to satisfy an essential condition. That is, the quaking regions separated by a gap of the width of one mesh should be divided into two clusters, as in cluster No.2 and No.3 in (a), in order to distinguish between the cases of (b) and (c) in S3 Figure that means to detect such small earthquakes as in EQ_C between the larger ones EQ_A and EQ_B . In other words, the clustering should not suffer from the bias toward convex clusters as k -means do (see⁵² and its extension to high dimensional data by reducing dimension⁵³), that means to obtain only such clusters as in case (c) of S3 Figure even if earthquakes between these clusters exist in the target data as (b) of S3 Figure. This difference is abstracted in S2 Figure. Approaches such as density- or grid-based clustering take denser regions than their surroundings as clusters, but do not fit the purpose here to unite regions, once separated by a boundary if the density on the boundary is weaker than the centroids of clusters but is being reinforced after. Although we may avoid the bias toward convex clusters by employing spectral clustering⁵⁵, its computational complexity is $O(n^3)$ that is not as simple as **make_clusters** where the complexity is $O(n)$. Pre-setting, as well as of k that should be set initially in k -means, is also required in hierarchical clustering where the depth of the hierarchy, meaning how clusters should be divided, is to be determined by a supplementary method or controlled interactively by the user watching the obtained tree.



S1 Figure. Clustering of quaking meshes in $Msh(S)$. Each cluster ($C_{x_0 y_0}$) grows as a subset of $Msh(S)$ by tracing neighboring quaking meshes from a seed ($m_{x_0 y_0}$), which is selected randomly from quaking meshes i.e., from $Msh(S)$, belonging to no cluster generated so far. Therefore, $x_0 y_0$, the suffix of the seed mesh, is used as the suffix of cluster $C_{x_0 y_0}$. This growth is halted when no new candidate of seed can be found. (** Linked from S1Text)



S2 Figure. Clustering by $\text{make_clusters}(S, t)$ in Step 1, compared with k -means for various k 's, for imaginary regions. (a) and (b) show the results of the presented **make_clusters** for different regions. In (a) and (b), each quaking (black) mesh belongs to the same cluster as another quaking mesh, as denoted by the same digit in this figure, as far as they touch via an edge or a vertex. The number of clusters is a result of the proposed algorithm from a sequence of earthquakes e.g., 3 for (a) and 5 for (b). On the other hand, (c) and (d) show the results of k -means for k set to 3 and 5 respectively for regions corresponding to (a) and (b). In (c), the largest cluster in (a) is separated into two, and the mesh isolated in (a) (the single-mesh cluster No.3) can join the enlarged cluster No.3 in the case of (c) because the mesh is close to the centroid of this cluster. Such a result in (c) is not acceptable in the proposed method, because the quaking regions separated by a gap of the width of one mesh, such as cluster 3 in (c) should be divided into two clusters, as in cluster No.2 and No.3 in (a). Furthermore, the uncertainty of belonging clusters for some meshes may occur in the iterative process of k -means algorithm, as in (d) where two meshes suffer from the equal distance to cluster 3 and 4, which also disturbs analysis. (** Linked from **S1Text**)

S2 Text: Dealing with Small Earthquakes

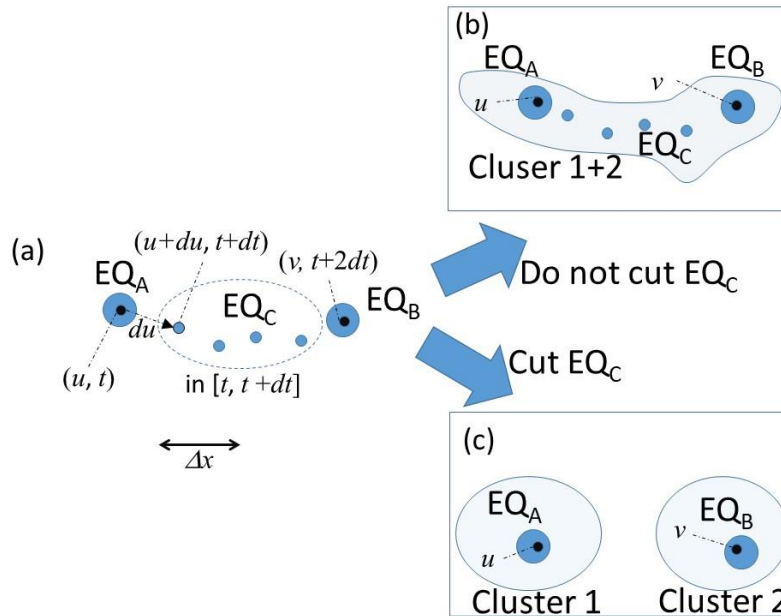
*Linked from **Data and Its Availability**

There is a possibility that the increase in the number of earthquakes may be just a transient change or aftershocks of a large earthquake. Studies on earthquake predictions often discount or cut aftershocks, regarding them as noises. However, in this paper, aftershocks should not be cut off for the reason below.

As in S3 Figure, suppose an earthquake EQ_A occurred at position u at time t , and a group of earthquakes as EQ_C occurred as aftershocks of EQ_A in the region, including position $u+du$ at $t+dt$, where du is a vector such that $|du| < \Delta x$ where Δx is the mesh size. Also suppose each earthquake in EQ_C occurred within distance Δx from some others in EQ_C , i.e., belonging to the same cluster as EQ_A . Then suppose a new earthquake EQ_B at position v at time $t+2dt$ occurred, belonging to this same cluster, as in (b) of S3 Figure, and that the shortest distance from v to one of the focal points in EQ_C is less than Δx .

Here note that EQ_C occurred from a cause common to EQ_A because EQ_C is a sequence of aftershocks of EQ_A . Thus, here, EQ_A , EQ_B , and EQ_C are regarded as to form one cluster, by regarding the line from u to v as a bridge of two sub-clusters (one including u , the other v). If we cut away earthquakes on this line only because they are small, we overestimate the regional entropy due to regarding one cluster sharing a common cause as two separate sub-clusters, biased to convex clusters as a result, as in Fig. S5 (c).

For example, in the case of earthquakes in Kumamoto prefecture in Japan (M7.3, 2016), the first shock of M6.5 corresponds to EQ_A , followed by a large number of small aftershocks as in EQ_C , and by the largest earthquake M7.3 corresponding to EQ_B . Furthermore, after a sequence of smaller earthquakes, the one of M5.3 occurred in the neighboring prefecture Oita. Among them, the first large quake EQ_A , the following largest EQ_B , and the one in Oita would be regarded to be in clusters of frequent earthquakes apart from each other, if the sequence of small earthquakes between them (as in EQ_C) had been cut away from the data.



S3 Figure. The reason why aftershocks should not be cut off here. Suppose earthquake EQ_A occurred at position u at time t , and a group of earthquakes as EQ_C occurred as aftershocks of EQ_A . Earthquakes in EQ_C occurred close to each other, and a new earthquake EQ_B occurred at position v close to EQ_C . EQ_A , EQ_B , and EQ_C can be regarded as in the same cluster. However, if we cut earthquakes in EQ_C , we overestimate the regional entropy, because the cluster gets separated into two as in (c). (** Linked from **S2Text**)

	10	20	30	40	50	60	70	80	90
J1995101923501350	038	281421	165	1303276	203	47	36	1211	7296NEAR AMAMI-OSHIMA ISLAND 17K
J1995101923541548	074	280705	196	1302082	315	36	19	121	7296NEAR AMAMI-OSHIMA ISLAND 3K
J1995101923550077	020	275286	052	1301313	097	46	18	121	7296NEAR AMAMI-OSHIMA ISLAND 3K
J1995101923554615	018	282183	075	1301641	071	2750069	19	111	7296NEAR AMAMI-OSHIMA ISLAND 3K
J1995101923564600	032	334716	330	1365902	4383	49	28	171	5208SE OFF KII PENINSULA 5S
J1995101923570077	046	281592	222	1301695	192	4413316	24	111	7296NEAR AMAMI-OSHIMA ISLAND 3K
J1995101923581581	046	275889	129	1301381	231	51	21	121	7296NEAR AMAMI-OSHIMA ISLAND 3K
J1995101923585659	083	280732	231	1302093	393	46	28	121	7296NEAR AMAMI-OSHIMA ISLAND 4K
J1995102000003024	029	280326	120	1300648	168	63	24	121	7296NEAR AMAMI-OSHIMA ISLAND 4K
J1995102000010462	060	280677	235	1302076	259	32	33	1212	7296NEAR AMAMI-OSHIMA ISLAND 11K
J1995102000013723	047	412495	114	1400202	121	3	09	121	1 16OSHIMA PEN REG HOKKAIDO 4K
J1995102000025381	060	422866	109	1390288	282	14	21	121	1 18SW OFF HOKKAIDO 8K
J1995102000050611	062	281062	182	1300210	268	22	20	121	7296NEAR AMAMI-OSHIMA ISLAND 3K
J1995102000055617	019	281336	096	1302258	082	2330145	24	111	7296NEAR AMAMI-OSHIMA ISLAND 3K
J1995102000061504	043	281669	214	1302405	174	4431382	27	111	7296NEAR AMAMI-OSHIMA ISLAND 3K
J1995102000074969	115	281066	272	1301816	506	31	32	1713	7296NEAR AMAMI-OSHIMA ISLAND 5S
Date and time		latitude		longitude		depth	magnitude		epicenter by the name of place

S4 Figure. The data structure in the earthquake catalog of JMA. Earthquakes of JMA magnitude (the two digits xy above means magnitude $x+y/10$) 2.0 or larger are dealt with, where magnitude values have been obtained by JMA. Source: Japan Meteorological Agency website (<http://www.data.jma.go.jp/svd/eqev/data/bulletin/hypo.html>). (** linked from **Data and Its Availability**)

Supplementary Table S1. The number of earthquakes of M2.0 or larger in the target. The target area is (25,125)-(45,145) in Fig.2, for each year in the target of the analysis. The total number for all years is 613136. (** linked from **Data and Its Availability**)

		1991	6473	2001	15908	2011	88562
		1992	8702	2002	15038	2012	35812
1983	4807	1993	13234	2003	20222	2013	24821
1984	4168	1994	15167	2004	21301	2014	21360
1985	3970	1995	25063	2005	19838	2015	19989
1986	4874	1996	16855	2006	15436	2016	33776
1987	5204	1997	16212	2007	17085	2017	7364
1988	5448	1998	16038	2008	18695		
1989	6537	1999	13773	2009	16015		
1990	6307	2000	32423	2010	16659		



S5 Figure. The distribution of earthquake intensity. The digits mean the intensity by the earthquake on 6th October 2000. Source: Japan Meteorological Agency website <https://www.data.jma.go.jp/svd/eqdb/data/shindo/Event.php?ID=156371> . (** linked from **The time series of clusters and RESI in Results**)

S3 Text: The Convenience of RESI for Dealing with Large Scale Land Crusts

** Linked from **Regional Entropy of Seismic Information**

Proposition: $Hr(S, t)$ is equal to the average of the values of regional entropy for all sub-regions of S .

Proof: Given sub-regions S_i of S for $i = 1, 2, \dots, N_S$, where N_S is the number of sub-regions of S . A sub-region corresponds to a cell in Fig.2. The entropy of region S , reflecting the distribution of earthquakes to clusters in S , is given as H in equation (S1). Here, $|S|$ represents the number of clusters in region S . C_{ij} represents the j -th cluster in sub-region S_i . Here, for simplicity, we assume each cluster is included properly in some sub-region i.e. not divided by boundaries of sub-regions. Hereafter, " $i \in (1, \dots, N_S), j \in (1, \dots, |S_i|)$ " is shortened to " i, j ."

$$\begin{aligned} H(S) &= - \sum_{i,j} p(C_{ij}|S) \log p(C_{ij}|S) \\ &= - \sum_{i,j} p(C_{ij})/p(S) \{ \log p(C_{ij}) - \log p(S) \} \end{aligned} \quad (S1)$$

Equation (S2) is obtained from Eq. (S1) using the equality of $p(C_{ij})$ to $p(C_{ij}|S)p(S)$ because C_{ij} is a proper part of S , and $p(S)$ to $\sum_{i,j} p(C_{ij})$.

$$p(S)H(S) = - \sum_{i,j} p(C_{ij}) \log p(C_{ij}) + p(S) \log p(S). \quad (S2)$$

On the other hand, entropy $H(S_i)$ for region S_i is given as

$$H(S_i) = - \sum_j p(C_{ij}|S_i) \log p(C_{ij}|S_i) = - \sum_j p(C_{ij})/p(S_i) \{ \log p(C_{ij}) - \log p(S_i) \} \quad (S3)$$

Here is used the equality of $p(C_{ij})$ to $p(C_{ij}|S_i)p(S_i)$ because C_{ij} is a proper part of S_i , and $p(S_i)$ to $\sum_j p(C_{ij})$. As a result, Eq.(S4) is obtained from equations (S2) and (S3).

$$\sum_i p(S_i) \{ H(S_i) - \log p(S_i) \} = - \sum_{i,j} p(C_{ij}) \log p(C_{ij}) = p(S) \{ H(S) - \log p(S) \}. \quad (S4)$$

Thus, we can say the RESI of S , represented by $Hr(S)$ and defined as $\{H(S) - \log p(S)\}$, is equal to the average of $Hr(S_i)$ for all sub-regions S_i of S for $i = 1, 2, \dots, N_S$, weighted by $p(S_i)$. Time t has been just cut above from equations for simplicity, so $H(S_i) - \log p(S_i)$ can be replaced with $Hr(S_i, t)$ according to equation (2), and $H(S) - \log p(S)$ with $Hr(S, t)$. Then, by substituting each S_i for all i with all S' that cover S , equation (S5) is derived.

$$Hr(S, t) = \sum_{S' \in S} p(S', t) Hr(S', t) / p(S, t). \quad (S5)$$

<EOP>

This proposition justifies the comparison of $Hr(S, t)$ for region S with $Hr(S^+, t)$ for region S^+ , the background region including S and its surrounding regions, because $Hr(S^+, t)$ can be obtained as the average of regional entropy of all regions included in S^+ , without any non-linear effect due to adding sub-regions out of S .

The LHS of equation (S4) corresponds to just subtracting $\sum_i p(S_i) \log p(S_i)$ from traditional conditional entropy $H(C|S_i)$ defined by $-\sum_{j \in |S_i|} p(C_{ij}) \log p(C_{ij}|S_i)$. This is the reason why $H(S) - \log p(S)$ of region S is here called the Regional Entropy i.e., entropy conditioned by region S , denoted by $Hr(S)$. Note regional entropy is about the spatial distribution of earthquakes, not the entropy of the energy distribution of earthquakes as in literature ⁴⁴. More generally, the entropy of a system in statistical physics has been known to be the sum, not the average as in this proposition, of entropies of the sub-systems of the system. This difference comes from our definition of regional entropy in which each earthquake belongs exclusively to one cluster, which belongs exclusively to one region.

S4 Text: The Outlines of Compared Baselines

** Linked from Measures for the Utility of RESI

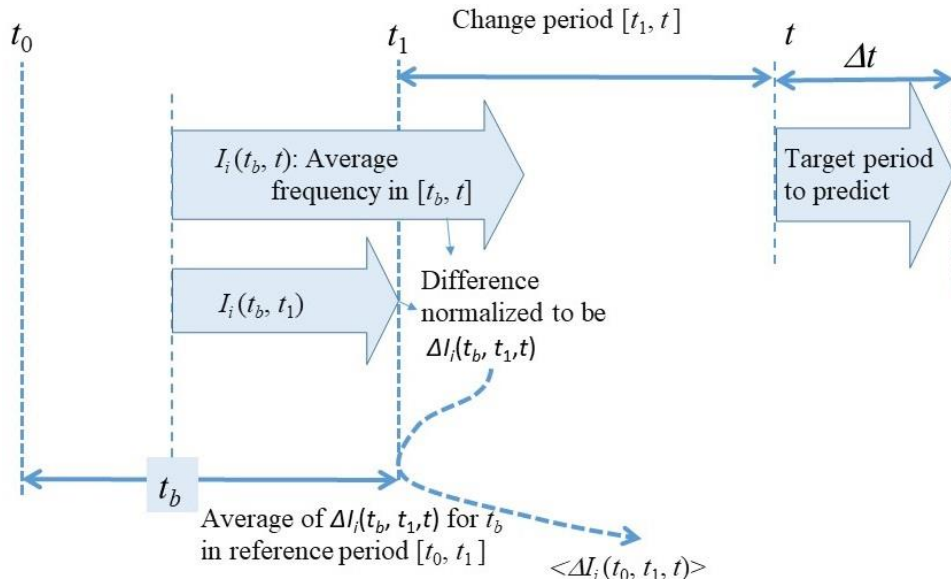
In this section, abstracts of Pattern Informatics and Relative Intensity, compared with the proposed index, are introduced to explain the usage of these methods in the experiments here. The details are referred to the original literature shown below.

Index in Pattern Informatics $PI(S_i, t_0, t_1, t)$

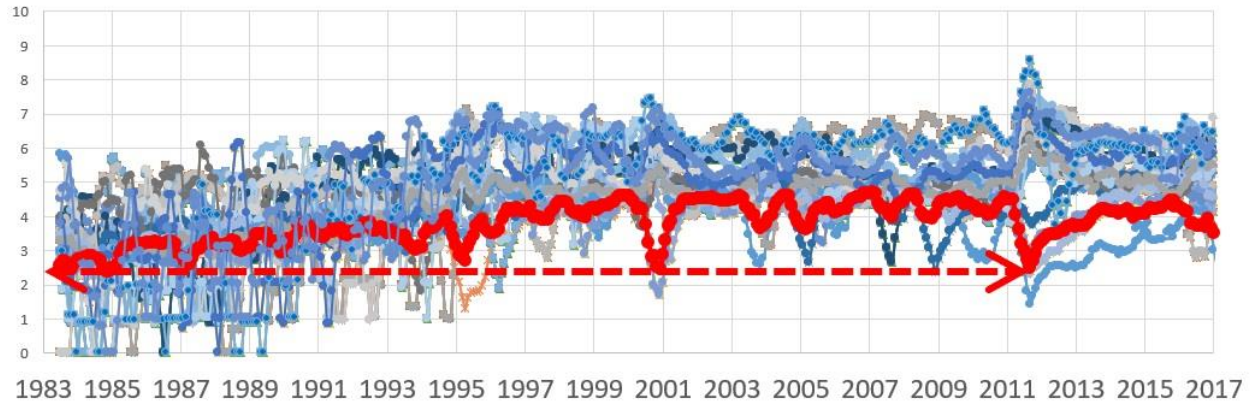
PI represents the risk of earthquakes in region S_i , represented by $\Delta PI(S_i, t_0, t_1, t)$ following the literature in pattern informatics (PI^{30,31}). Here, as illustrated in S6 Figure, $[t_0, t_1]$ is the reference time range in the past, and $[t, t + \Delta t]$ is the target period (1 year) to predict the risk. For each time t_b in $[t_0, t_1]$, the average frequency of events above a defined cutoff (M_θ is set to 2.0, for a fair comparison with RESI) from t_b to t is obtained. This average frequency is normalized (i.e., divided by the standard deviation for all regions S_i for all i , after subtracting the average for all S_i) to obtain $I_i(t_b, t)$. Then $\Delta I_i(t_b, t_1, t)$ is obtained as $I_i(t_b, t) - I_i(t_b, t_1)$. The average of $\Delta I_i(t_b, t_1, t)$ for all t_b in $[t_0, t_1]$ is computed to obtain $\langle \Delta I_i(t_b, t_1, t) \rangle$. Finally, $\langle \Delta I_i(t_b, t_1, t) \rangle$ is squared and its difference from the background value (average for all S_i in the given map) is obtained as $PI(S_i, t_0, t_1, t)$ where t_0 and t_1 are set to be Jan 1983 and Jan 1987 respectively in this paper. Summarizing this method, the risk in the period $[t, t + \Delta t]$ in region S_i is estimated as the change in the earthquake risk for the recent period from t_1 and t .

Relative intensity $RI(S_i, t_0, t_1, t)$

For each time t , RI (for details see^{34,36,39}) here is given by $n_i(t_0, t_1, M_\theta) / \sum_{S_j \in S} n_j(t_0, t_1, M_\theta)$. Here, $n_i(t_0, t_1, M_\theta)$ is the average number of earthquakes in the cells including S_i and the adjacent cells surrounding S_i . M_θ is the cutoff magnitude and t_0 and t_1 are times before the target time (year or month) t to predict earthquake risk (precisely $[t, t + \Delta t]$ is the target period by setting Δt to the period length). S is the set of all the cells in the given map corresponding to the data analyzed. In applying RI in this paper, t_0 and t_1 have been said to be ideal if $t_1 - t_0$ is set large³⁹, so here we set t_0 as 1983 and t_1 as $t - 1$.

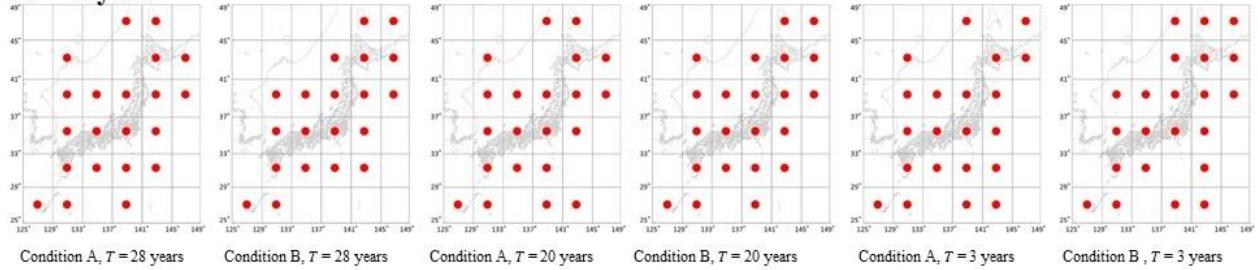


S6 Figure. Computing $\langle \Delta I_i(t_0, t_1, t) \rangle$ in obtaining $PI(S_i, t_0, t_1, t)$ in Eq.(12). PI is the index in pattern informatics, that is here compared with $Hr(S_i, t)$, where $[t_0, t_1]$ is the reference period and $[t, t + \Delta t]$ is the target period of which the risk of earthquakes should be predicted. $\langle \Delta I_i(t_0, t_1, t) \rangle$ above is squared and its difference from the background value (average for all S_i in the given map) is obtained as $PI(S_i, t_0, t_1, t)$ for t_0 and t_1 set to 1983 and 1987 respectively. Note: the symbols used here differ from those in the references. For example, t was shown as t_2 in the literature²⁷. (** Linked from S4Text)

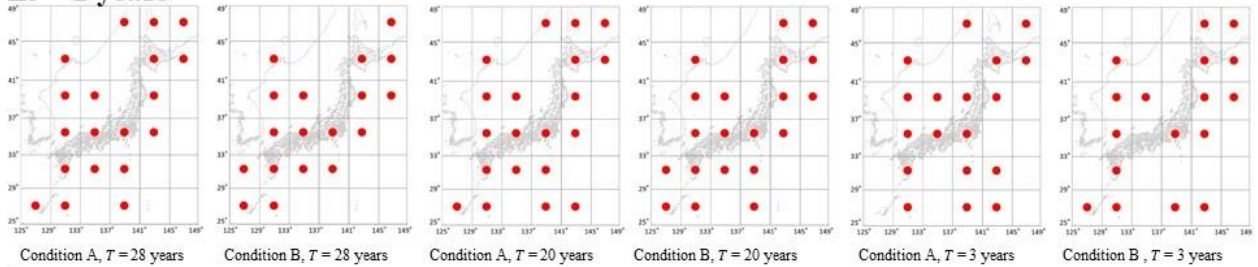


S7 Figure. The monthly transition of RESI for all regions and all Japan. $Hr(S, t)$ for all S i.e., 36 regions, corresponding to cells in Fig.2 for the background blue thin curves. The thick red curve is obtained as the average of the 36 regions, on Eq.(S5) in S3 Text, i.e., the value transition of RESI for the whole map of 36 regions. We find the monotonous increase of the overage for at least 28 years as in the arrow. (** Linked from **Discussions**)

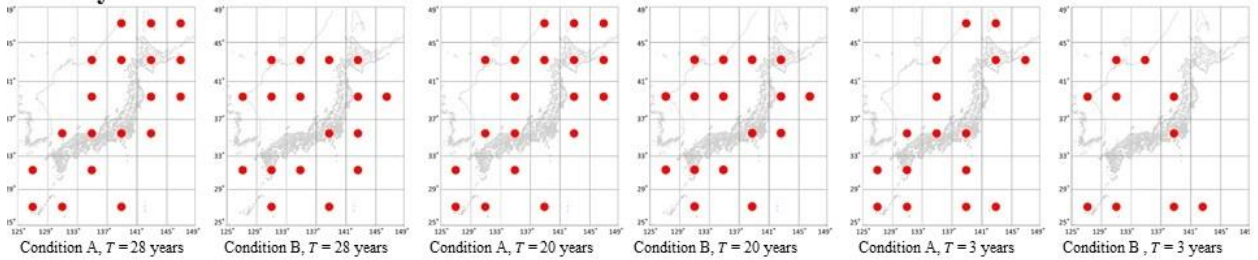
$\Delta t = 1$ year



$\Delta t = 2$ years



$\Delta t = 3$ years



S8 Figure. The performance of the compared alarming functions. This alarming functions $Hr(S, t)$, are compared for setting Δt to 1 year, 2 year, and 3 years respectively in (a), (b), and (c) here, setting T in Eq.(3) to 3, 20, and 28 years. The result did not change for setting T any longer (T is shorter than 35 years that is the period of the available data) The red dots in a cell mean the same as in Fig.6. Source of the background map: Japan Meteorological Agency website (<http://www.data.jma.go.jp/svd/eqev/data/intens-st/>) (** Linked from **Discussions**)

S5 Text: The Method for Evaluating Alarming Functions

**** Linked from Measures for the Utility of RESI**

This section is presented for explaining the reason for choosing the evaluation criteria of Eq.(7) and (8) in the comparison of RESI with baselines. Here, let us show some possible alternative methods for evaluation, and discuss the advantages and disadvantages.

An alternative of RESI, as a value changing time with similarity to the activation of earthquakes, is to take the point-to-point similarity of two sequences (f : alarming function, g : earthquake activity), where the times of the corresponding points in the two series may not always correspond exactly. This evaluation may be executed by using Dynamic Time Warping (DTM)⁶⁰, of which the availability as an existing tool is an advantage. However, in this paper, the aim is to evaluate not only the similarity but also the correlation by an advance time within a given length (Δt), of precursory alarms obtained by the alarming function to the activation of earthquakes that are the target of prediction. Therefore, the criteria in Eq.(7) and (8) are chosen here where the correlation is evaluated within the preceding and the delay of Δt respectively.

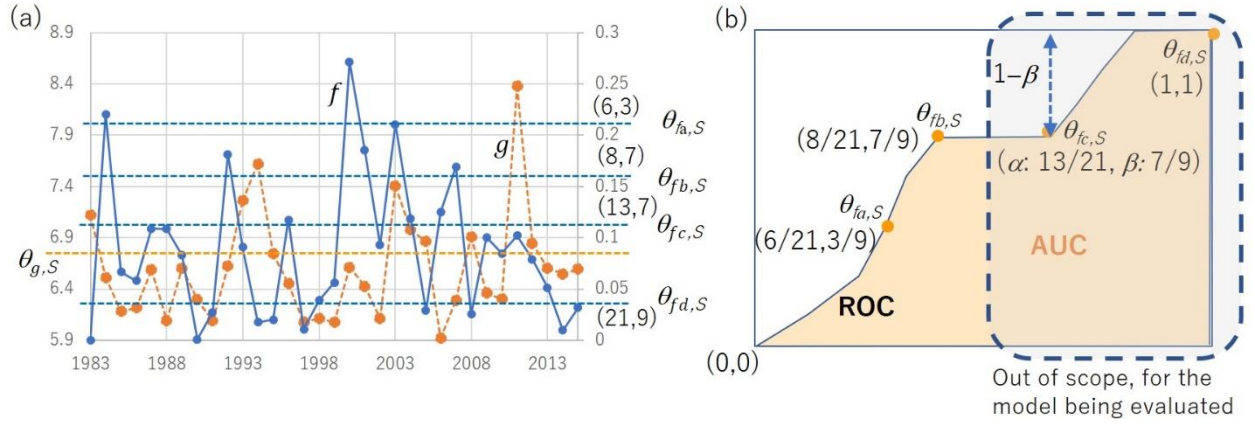
Another prevalent evaluation measure is the correlation of the alarms with the real activations, with tolerant delay, as in the literature¹⁶. For example, the rate of error (such as false positive) and the advance time i.e., the precedence in the word in this paper, of the obtained alarm has been measured⁵⁸. On the other hand, the purpose of evaluation in this paper is to investigate the correlation of function f representing the alarm of precursor, within a given advance time of precedence, with g representing the real activation of earthquakes. In order to fit this purpose, the criteria in Eq. (7) and (8) are used for evaluating the correlation with a tolerant delay Δt or with an advance (precedence) time Δt , for a given Δt (1 or 2 years in the evaluation in this paper).

The Area Under Curve (AUC) of Receiver Operating Characteristic (ROC^{16,59}) has been also employed as a measure of an alarm's correspondence to the target event, that integrates the evaluations for various values of threshold θ_f , over which high_ f used in Eq. (7) and (8) for each alarming function f (Hr, PI, and RI in this paper) takes the value of 1. In computing AUC, θ_f is set to various values, for which the probability of high_ f ($f > \theta_f$) \wedge high_ g ($g > \theta_g$) is given as Y , and of high_ f \wedge not high_ g as X respectively in a two dimensional curve, the area under which i.e., where Y is less than on the curve, is computed as AUC (see S9 Fig). Increasing θ_f here means to reduce θ_{std} in Eq.(3). Let us show why AUC is not used as the evaluation measure here.

Let g denote a function quantifying the activity of earthquakes that has a peak at time t_g . By increasing θ_f over a certain value θ_{fa} , we may get only a small number (such as three) of peaks of f . This makes an unreliable estimation of the correlation between alarm function f and the prediction target g , because the correlation is affected substantially by the choice of one from two peaks t_{f1} and t_{f2} of f . For example, if $f(t_{f1}) > \theta_f$ and $f(t_{f2}) < \theta_f$, and $t_{f1} < t_g - \Delta t$ and $t_g - \Delta t < t_{f2} < t_g$, no correlation between the two peaks of f and the peak of g at t_g will be obtained. On the other hand, if $t_{f2} < t_g - \Delta t$ and $t_g - \Delta t < t_{f1} < t_g$, the preceding correlation of the peak of f at t_{f1} with the peak of g at t_g results in the increase of a positive value to $\text{prec}(f, g, S, \Delta t)$ in Eq.(7). Such an effect due to a small difference of peaks, i.e., $f(t_{f1})$ and $f(t_{f2})$, even if it is due to noise, causes to change $\text{prec}(f, g, S, \Delta t)$ substantially if the number of all peaks is small. Such a case is not ignorable in the sequence of RESI values, because close values of $\text{Hr}(S, t)$ tend to appear near the time of saturation.

On the other hand, suppose there are B times where high_ g (high_ g = 1) and A times of not high_ g (high_ g = 0) in total. By setting θ_f down to a certain value, we may obtain the times of high_ f to cover βB times of high_ g and αA times of not high_ g within a delay of Δt from any time of high_ f , for α and β in $[0, 1]$. Then, the obtained ROC should include (α, β) which means the proportion of $1 - \beta$ of all the times of high_ g are not covered unless θ_f is set to a lower value (AUC comes to be smaller for a large $1 - \beta$). However, because $1 - \beta$ decreases discontinuously with the increase in θ_f , the change of AUC fails to fit the basic assumption of AUC that the ROC is a convex curve. That is, the right end part in S9 Figure is unreliable. Thus AUC cannot be regarded as a reliable evaluation measure for use in this paper.

For avoiding these problems of AUC based evaluation, we chose to fix the threshold of peaks by θ_{std} in Eq.(3), rather than integrating various thresholds to evaluate AUC. And, putting activation(S, t) as g , $high_g(S, t)$ is set to 1 if $g(S, t)$ is significantly larger than average and $g(S, t)$ is the largest in the time range of $[t-2 \text{ years}, t]$, as stated in Measures for the Utility of RESI, for detecting the precursors of activation that lasts a few years.



S9 Figure. ROC/AUC, if applied, for an imaginary example. The threshold $\theta_{f,S}$ is varied, fixing $\theta_{g,S}$. Among all times within Δt (e.g., 3 yrs) from a time f was of $high_f$ (i.e., over $\theta_{fa,S}$, $\theta_{fb,S}$, $\theta_{fc,S}$, or $\theta_{fd,S}$ for each setting of $\theta_{f,S}$), digits i and j in (i, j) in (a) are respectively the numbers of times when g was and was not of $high_g$ i.e., over $\theta_{g,S}$. Each dot in (b) shows the position (X, Y) obtained as $(i/21, j/9)$, where 21 and 9 are all times of $high_g$ and other times in the target period of 30 years (1985 to 2015: note the first three years 1983-1984 are cut when 2 years preceding of f from g is evaluated). (** Linked from S5 Text)